Study of the life cycle of tropical cloud and precipitation systems using MTSAT-1R and TRMM data

（運輸多目的衛星 MISAT-1R および熱帯降雨観測衛星 TRMM データを用いた

熱帯域の雲降水システムの発達過程に関する研究）

Keiji Imaoka

（今岡　啓治）

Study of the life cycle of tropical cloud and precipitation systems using MTSAT-1R and TRMM data

（運輸多目的衛星 MISAT-1R および熱帯降雨観測衛星 TRMM データを用いた

熱帯域の雲降水システムの発達過程に関する研究）

Keiji Imaoka

（今岡　啓治）

A dissertation for the degree of Doctor of Science
Department of Earth and Environmental Sciences,
Graduate School of Environmental studies,
Nagoya University
(名古屋大学大学院環境学研究科地球環境科学専攻学位論文　博士（理学）)

2013

Abstract

Observations from the Multi-functional Transport Satellite (MTSAT)-1R and the Tropical Rainfall Measuring Mission (TRMM) satellite are analyzed to show the statistical view of the cloud life cycle, including the changes of vertical structure of rainfall, over the Maritime Continent and a part of the tropical western Pacific. The analysis focuses on the isolated cold cloud systems, which can be considered as fundamental self-organized cloud systems. After identifying temporally connected isolated cold cloud systems by a cloud tracking procedure, spatiotemporally synchronized TRMM observations with the cloud systems were searched and various statistics were computed. Clear life cycle changes of the average reflectivity profile from the Precipitation Radar (PR), such as those of radar echo height and the bright band feature, are statistically confirmed over the ocean area. The long-lived systems in this analysis show a behavior similar to those of typical mesoscale convective systems. The systems start from the intermediate phase between initial and mature stages, reach the mature stage with the maximal cloud and precipitation areas at the mid-period of the lifetime, and decay. The increase of precipitating area is mostly attributed to that of stratiform precipitation. The rain rate and the radar echo height indicate their peak during the early hours and decrease with elapsed time. Precipitation-size ice particles and the higher ratio of lightning-accompanied systems are observed during the early elapsed time, and their peaks seem to synchronize with the peak of the convective-conditional average rain rate. In contrast, short-lived systems in this analysis decay rapidly and do not produce an extension of cloud and precipitation. It is speculated that the systems are already in the mature stage when they are identified, from the observations of higher ratio of stratiform rainfall area and clearer feature of bright band than those of long-lived systems at the time of system formation. The results also show that the difference between rainfall estimates of the TRMM Microwave Imager

(TMI) and PR depends on the phase in the lifetime. TMI tends to provide higher conditional average rain rates at mature phase than that of PR. Also, the cold cloud area with an IR brightness temperature threshold of 235 K, which is the basis of the GOES Precipitation Index, does not track the life cycle changes of total rain volume, probably because it mainly reflects the areas of stratiform precipitation and anvil clouds, particularly in the middle and later stages of the long-lived systems. To understand the life cycle of latent heating profiles and its effect on the surrounding atmospheric field, similar statistical analysis is performed for the latent heating profiles derived from the PR rainfall profiles over the isolated cold cloud systems. Clear life cycle variations are confirmed for convective heating profiles, while those in stratiform heating profiles are negligible. The resulting total heating profiles show the heating at all levels during the lifetime and the peak shifts from 5 to 8 km with elapsed time. Because the stratiform rainfall area and its life cycle variations are large, the total heating contribution released by a cold cloud system to the surrounding atmosphere is dominated by changes in the rainfall area and the ratio of the stratiform rainfall, rather than by changes in the shape of convective heating profiles.

Contents

List of Figures

1. Introduction

The life cycle of cloud and precipitation systems has been an important research topic in the field of atmospheric science. Although in this field, there are a number of case studies that use ground-based radar observations and model simulations, and the basic concept of the cloud life cycle may be recognized well, global-scale systematic investigation is not sufficient. Organized and larger cloud systems, which are major sources of precipitation, are composed of emerging and dissipating convective systems known as mesoscale convective systems (MCSs). Therefore, knowing the life cycle characteristics of each convective system forms the basis of understanding the behavior of the organized systems. Moreover, recent studies have revealed the relationship between uncertainties in rainfall estimates and the development stage of the cloud system (e.g., Rajendran and Nakazawa 2005). Precise and comprehensive understanding of this relationship will help improve precipitation estimates from various remote sensing instruments. Since these instruments utilize different physical principles of interaction between precipitating clouds and electromagnetic waves, their sensitivities depend on the cloud life cycle.

Geostationary infrared observations with cloud tracking methods have been widely used in cloud life cycle analysis, such as by Williams and Houze (1987), Mapes and Houze (1993), Chen and Houze (1997), Machado et al. (1998), Mathon and Laurent (2001), and Kondo et al. (2006). Machado et al. (1998) reviewed previous studies in terms of the effect of selection of the tracking method and the threshold of brightness temperatures (Tbs) on the resultant cloud life cycle statistics. They found that most life cycle statistics were less sensitive to the tracking method used if the time resolution of the satellite observation was high enough to track the evolution of the system. Kondo et al. (2006) tested two tracking methods known as the area overlap technique and the minimum speed technique, which utilize the widest

overlapping area and the smallest relative moving velocity between two cloud systems in consecutive satellite images, respectively, for identifying the temporally connected cloud systems. On the basis of the result of comparison between the two techniques, Kondo et al. decided to use the minimum speed technique in their study, in which a small threshold of cold cloud area of 1963 km^2 was used. The selection of the minimum Tb threshold differs depending on the purpose of the study, as summarized in Mapes and Houze (1993). For example, a very low Tb threshold of 208 K is chosen to delineate heavy convective regions (e.g., Mapes and Houze 1993), and multiple thresholds are used to cover a wider area comprised of a warmer envelope with colder cloud cores (e.g., Boer and Ramanathan 1997 and Futyan and Del Genio 2007). For precipitation estimates, a threshold of 235 K has been widely used for the Geostationary Operational Environmental Satellite Precipitation Index (GPI), as described by Arkin and Meisner (1987). This technique has been employed to produce the infrared estimate of rainfall in the Global Precipitation Climatology Project (GPCP) monthly precipitation analysis, as described by Huffman et al. (1997) and Adler et al. (2003).

Geostationary orbiting satellites provide the most frequent observations over a specified longitude range and enable tracking of the temporal trajectories and evolution of cloud systems, even though the measurement method is currently limited to optical and infrared observations, in which the available information is obtained mainly from the upper layer of clouds. In contrast, lower orbiting satellites, which generally alleviate problems such as spatial resolution and active instrument transmission power, can be equipped with various remote sensing instruments, although the observation by each satellite is intermittent by nature. Therefore, geostationary and lower orbiting satellite systems are highly complementary, and their synergistic use is an important source of new information. In particular, use of the Tropical Rainfall Measuring Mission (TRMM), which introduced a new

era of wide-area rainfall measurement from space, provides unique opportunities. As the first of its kind in space, the Precipitation Radar (PR) has played a critical role in measuring the three-dimensional structure of tropical rainfall in conjunction with other valuable instruments onboard TRMM. In recent years, satellite observations have been used to retrieve latent heating profiles from precipitating cloud systems (Tao et al. 2006). It is widely accepted that latent heat released by condensation plays an essential role in cloud evolution. The important role of the heating profiles associated with typical MCSs in producing large-scale dynamics of the atmosphere (Hartmann et al. 1984; Schumacher et al. 2004) has also been recognized. Kondo et al. (2006) investigated the relationship between the evolution stage of cloud systems and collocated TRMM precipitation parameters. They found that rain rates from the TRMM Microwave Imager (TMI) and PR show maximum values at the time of minimum Tb or earlier. Futyan and Del Genio (2007) investigated the life cycle of MCSs over Africa using a cloud tracking methodology and compared this with observations from PR and the Lightning Imaging Sensor (LIS) on TRMM. Their results suggested fundamental differences between the convective life cycles over land and the ocean, which were consistent with previous studies in terms of differences in convective sustainability. Siqueira et al. (2005) used the International Satellite Cloud Climatology Project dataset and the TRMM products to identify and describe structural characteristics of convective systems over continental South America related to cold-frontal incursions in a 3-year period. Some studies, such as by Rajendran and Nakazawa (2005), shed light on differences in precipitation estimates among the various techniques and their relationships with cloud life stages. In addition, new ideas regarding the cloud life cycle are being investigated; for example, Inoue et al. (2009) used cirrus clouds ratio in a split window technique to identify cloud life cycle stages and compared the results with TRMM data, Mapes et al. (2009) compared MCS life cycles detected by infrared observations with wind divergence and vorticity derived from

scatterometer data and microwave total precipitable water, and Masunaga (2012) proposed a statistical approach for combining multiple low Earth-orbiting satellite observations to study the evolution of composite temperature and humidity fields on an hourly basis before and after the convection genesis. These studies enhance our comprehensive understanding of the cloud life cycle by investigating not only the cloud system itself but also the environment that controls the evolution of cloud systems.

This dissertation describes the results of a combined analysis of the cloud life cycle by utilizing the geostationary satellite and TRMM data. This study examined the cloud life cycle and its relationship with precipitation-related parameters such as rain rates, precipitating areas, rainfall types, radar reflectivity profiles, and lightning flashes. Also, heating profiles of precipitating clouds were evaluated to investigate the life cycle changes and the effect on the surrounding atmospheric field. To obtain a clear statistical view of the life cycle for the fundamental unit of the convective system, isolated cold cloud systems, without any splitting and merging processes, were identified by a cloud tracking method over the Maritime Continent and a part of the tropical western Pacific and used for the further statistical analysis.

2. Data and Methodology

2.1 Instruments and data

Approximately four years (June 2006–May 2010) of satellite observations were used over a rectangular region of 20°S–20°N and 90°E–180°W, which includes the Maritime Continent and a part of the tropical western Pacific as shown in Fig. 1. This study area is identical to that of Kondo et al. (2006). Since this area is situated between the Tropic of Cancer and the Tropic of Capricorn, the area is hereinafter referred to as tropical region. The satellites and instruments that provide data for this study include the Japanese Advanced Meteorological Imager on the Multi-functional Transport Satellite (MTSAT)-1R (Kigawa 2001) and three instruments, PR, TMI, and LIS, on the TRMM satellite. MTSAT-1R is a geostationary meteorological satellite developed and operated over longitude 140°E by Japan Meteorological Agency (JMA). Since the time MTSAT-2 satellite began its operational observation in July 2010, MTSAT-1R has been operating in standby mode. The TRMM satellite was launched in November 1997 into a non-sun-synchronous orbit with a 35° inclination and an altitude of 350 km. PR is the first ever precipitation radar in space operated in the Ku-band (13.8 GHz), developed by the Japan Aerospace Exploration Agency (JAXA) in cooperation with the National Institute of Information and Communications Technology (NICT) (Kozu et al. 2001). After the orbit boost performed in August 2001 to conserve fuel to maintain its orbit, the satellite altitude was increased from 350 km to 402 km. The swath width, horizontal and vertical resolutions, and minimum detectable echo are 250 km, 5.0 and 0.25 km, and 20.7 dBZ, respectively (Takahashi and Iguchi 2004). TMI is a NASA-developed 9-channel passive microwave radiometer across the frequency range of 10–85 GHz (Kummerow et al. 1998). TMI's swath width and horizontal resolution at 85 GHz after the satellite boost are 878 and 5.1 km, respectively. The LIS instrument is a staring optical

imager that detects optical pulses from lightning flashes during both day and night. It was designed and manufactured by NASA's Marshall Space Flight Center. The horizontal resolution and detection efficiency are about 5 km and 85%, respectively, and no corrections were applied for this efficiency in out study. More detailed information on the instrument and its performance validation can be found in Christian (1999) and Boccippio et al. (2002).

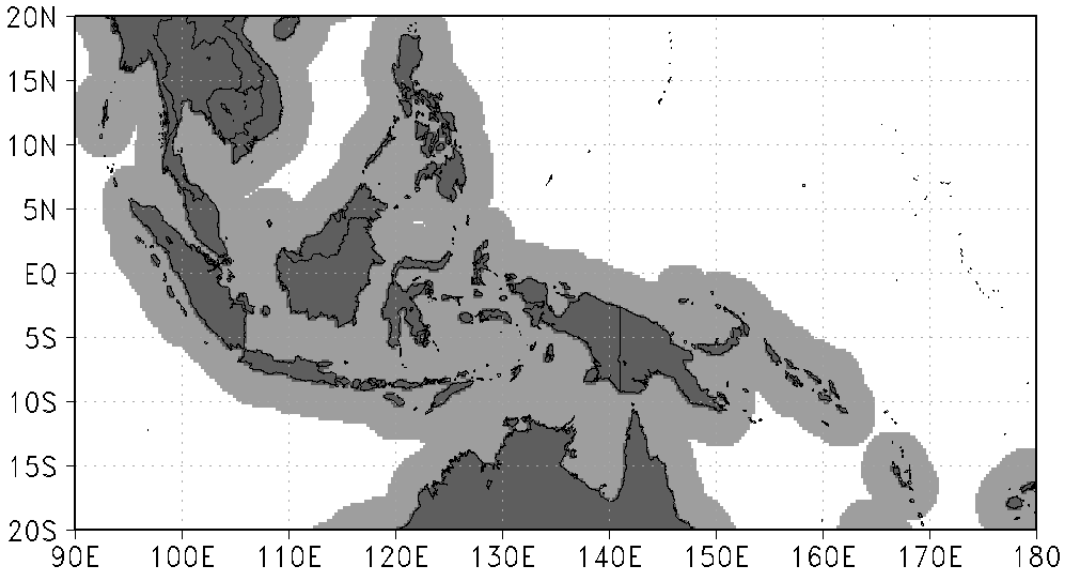

FIG. 1. Target area of present analysis. Dark gray, light gray, and white area indicate land, coastal ocean, and open ocean areas, respectively.

To identify cold cloud systems, gridded data of the IR1 (11 μm) infrared channel of MTSAT-1R were used. The grid size and temporal resolution were 0.04° and 1 h, respectively. The data were re-gridded into 0.1° resolution by a simple averaging method before applying the cloud tracking procedure by Kondo et al. (2006) described in the later section. The reason why we re-gridded into 0.1° resolution was to utilize the existing cloud tracking procedure as is and to ensure consistency between the results of Kondo et al. (2006) and the present study. Although the pixel distortion effect becomes pronounced particularly at the western edge of the study area, it may not produce serious effects on computing the areas of cold cloud systems since the size of enlarged pixels is comparable with the grid size we used. Data from TRMM PR were used to investigate life cycle changes of rainfall, rain type, and vertical profiles of radar reflectivity, rainfall, and heating rates. The TRMM 2A25 version-6 product (Iguchi et al. 2009), which includes information such as the attenuation-corrected radar reflectivity profiles, precipitation profiles, and precipitation types, was used in this study. Non-grid (orbital) files of the version-02 latent heat research product from PR based on the Spectral Latent Heating (SLH) algorithm (Shige et al. 2004, 2007) were also used. The SLH algorithm used in the version-02 heating profile product utilizes a lookup table produced from the Tropical Ocean and Global Atmosphere Coupled Ocean-Atmosphere Response Experiment simulations. This lookup table relates the statistically optimum heating profile to the precipitation top height and rain rate at the melting layer for convective and deep stratiform rainfall, respectively (Shige et al. 2004). Therefore, despite a lack of PR sensitivity to the small ice-phase hydrometeors in the anvil clouds, the algorithm can continuously track heating profiles throughout the cloud life cycle, with the exception of those in old convective cells without rainfall at the melting layer. In addition, universality of the lookup table was investigated by Shige et al. (2007) for the rainfall over oceans. After making several improvements, they reported reasonable performance of the SLH algorithm

through consistency check by using true heating profiles produced by the cloud resolving model and comparison between the retrieved profiles from PR and those derived diagnostically from the South China Sea Monsoon Experiment sounding data. The latent heat research product includes the net latent heating by the phase change of water and the difference between the apparent heat source and cooling/heating rate associated with radiative processes (Q_1-Q_R, hereinafter Q_{1R}). In this analysis, we used the Q_{1R} estimate as a diabatic heating rate. Synchronized observations by TMI provide the temporal changes of the TMI-estimated surface rain rate and the microwave scattering signature during the life cycle. In this study, we utilized the TRMM 1B11 version-6 product for Tbs and the 2A12 version-6 product for surface rain rates. The LIS instrument provides the frequency of lightning occurrence over the cold cloud systems and its relationship with the life cycle. The number of lightning flashes and their observed time in the LIS Science Data were used to obtain the lightning flash rate.

2.2 Analysis methodology

To track and identify the cold cloud systems, we applied the method and program used by Kondo et al. (2006). The program uses the minimum speed technique in which two systems with minimum relative moving velocity are identified as the same system. Another well-used method is the area overlap technique, in which consecutive cloud systems with the widest overlapping area are identified as the same system (e.g., Williams and Houze 1987; Mathon and Laurent 2001). The parameters used for the minimum speed technique include the maximum velocity of 100 km h^{-1}, IR1 Tb threshold of 235 K, and minimum cold cloud area corresponding to the area of a circle with a radius of 25 km. We first applied the temperature and area thresholds for hourly IR1 grid data with 0.1° resolution, and then identified

temporally contiguous cold cloud systems using the minimum speed technique. Emergence and dissipation were defined when no cold cloud region existed in two consecutive hours within 100 km. This study intends to present a clear statistical overview of the cloud life cycle for the fundamental self-organized cloud systems. Therefore, we focused on isolated cloud systems without any merging and splitting processes to prevent introducing additional complexities that may hinder our understanding of the characteristics of the life cycle. Although this reduced the number of target cloud systems and their sizes, it still secured the universality in discussing the typical cloud life cycle for small and short-lived systems as discussed by Kondo et al. (2006). It should be noted that the cold cloud systems, identified by the cloud tracking procedure with an IR Tb threshold of 235 K, do not indicate the whole life cycle stages, but may represent the stages from the intermediate between initiation and mature to dissipating. Although this analysis does not provide the information on cloud systems at the initiation stage, it still reveals the characteristics in considerable range of life cycle stages in terms of cloud evolution. Local time (LT) was calculated for each cold cloud system using Coordinated Universal Time (UTC) of the data and the central longitude of the system. Although it takes about 21 minutes for full–disk observation and about 10 minutes for our study area, we used the center time of each hourly grid data.

After identifying the cold cloud systems throughout the target period, spatiotemporally synchronized TRMM data with the cloud systems were searched and various statistics were computed. Since we used the hourly IR1 data, the temporal synchronization was limited within ±0.5 h. The statistics were sorted according to several conditions including the lifetime of the cold cloud systems defined by IR1 observations, elapsed time from the formation of the systems, and the surface condition. Regarding the surface condition, we categorized the identified cold cloud systems into those occurring over land, coastal ocean, and open ocean, as indicated in Fig. 1. To categorize surface types, we used a 0.25–degrees resolution gridded

dataset of land area ratio in a grid. A grid with a land area ratio of 25 % or larger is categorized as land. This dataset was originally created from the Global 30 Arc Second Elevation Data Set or GTOPO30 provided by the U.S. Geological Survey. The coastal ocean area was defined as the ocean region from the coast up to 300 km. Cross-boundary systems between different surface conditions during the lifetime were excluded from the statistics to avoid the characteristic blending, unless otherwise noted. Since the swath width of PR, which is about 250 km after the satellite boost, is the narrowest among the instruments, we selected only those cold cloud systems that were completely covered by the PR swath width. In calculating various areas, average values, and ratios, except the vertical information of PR, data were preprocessed into 0.1° resolution grids, which was consistent with the IR1 grid size.

3. Results

3.1 Characteristics of identified cold cloud systems

Before describing the results of the TRMM observation statistics, we must clarify the characteristics of the identified cold cloud systems using the cloud tracking procedure to correctly understand the nature of the statistics. Figure 2 shows the statistics of the mean cloud radius during the lifetime and the number of cloud systems sorted, relative to the lifetime during the analysis period. The total number of systems is 306,644. More than 90% of the systems have a lifetime between 1–5 h and relatively small systems are identified with a mean radius of about less than 40 km for 5 h lifetime systems. As described in Kondo et al. (2006), the number of systems decreases nearly exponentially with their lifetime. In this analysis, the relationship is expressed as

$$\log N = -0.20 \times T + 5.26 , \quad (1)$$

where N is the number of systems and T is their lifetime in hours. The same relationship during the period from June 2007 to August 2007 is similar to that in Kondo et al. (2006) for the data obtained by the Geostationary Meteorological Satellite (GMS) during the same period of 2000. This indicates the reproducibility of the cloud tracking result for the different sensor systems and data period. From the statistical characteristics of the systems shown in Fig. 2, we focus on the statistics of the TRMM data for lifetimes between 1 and 5 h, because the majority of the systems are in this lifetime range. It is said that typical isolated cloud system has a lifetime of several hours. An e-folding time, which corresponds to an average lifetime of an exponentially decreasing population, is approximately 3 h from (1). Therefore,

it is considered meaningful to investigate characteristics and differences of the systems with lifetimes shorter or longer than 3 h. On the basis of this idea, results will be shown and discussed for 2 h lifetime systems and 4 or 5 h lifetime systems in later sections. From the minimum area threshold used in this analysis, it is evident that the systems are not individual cumulonimbus. On the other hand, the typical MCSs found in studies such as Houze (1993), Houze (2004), and Nesbitt and Zipser (2003) have comparable or larger sizes than those of the systems in this study with lifetimes of 1–5 h (about 5000 km^2).

Geographical distribution of the cold cloud systems is shown in Fig. 3a for different LT of the day. Also, the diurnal variation of the number of cold cloud system occurrences is shown in Fig. 3b for open ocean, coastal ocean, and land areas. Fig. 3b is shown in the form of the probability density function (PDF), in which the number of occurrences is normalized by the total number for each surface type. In Fig. 3b, cross-boundary systems between open ocean and coastal ocean (coastal ocean and land) are categorized as the systems over open ocean (coastal ocean). The time of occurrence is defined by the center of the lifetime. From the exponential relationship between the lifetime and the number of systems in Fig. 2, the number of occurrences in Figs. 3a and 3b is dominated by shorter lifetime systems. However, since our visual comparison of the same figures for different lifetimes does not indicate significant differences, we believe that the main characteristics in Figs. 3a and 3b is not distorted. About 5% of the MTSAT-1R images at 1400 UTC are missing or not used in this analysis because of the erroneous data included. Cold cloud systems with a lifetime longer than 2 h, however, can be detected even with the 1 h data missing, since emergence and dissipation are defined when no cold cloud region exists in two consecutive hours as already mentioned. Although 1 h lifetime systems at 1400 UTC can not be detected, the ratios of the number of missing systems to the total are about 2% and 0.5% in 1 h and 4 h time bins, respectively. In general, cold cloud systems tend to occur more frequently over land, coastal

ocean areas, and some open ocean areas such as around the Inter-Tropical Convergence Zone (ITCZ) and the South Pacific Convergence Zone (SPCZ). Clear diurnal variations can be seen in the location of the systems, particularly over and around the Maritime Continent. Over land, the number of occurrences is lowest during 0800–1200 LT, increases and reaches its maximum during 1200–1600 LT, and gradually decreases during 1600–2000 LT. The increase appears to begin from the coastal and mountainous areas and extends into the inland areas. Such diurnal patterns are most evident over the island of Borneo. Over the coastal ocean areas, the number of occurrences seems to be low during 1600–2000 LT and 2000–2400 LT, when the occurrence frequency over land reaches a peak and decreases. In subsequent night and morning hours until 0800–1200 LT, a moderate increase in number of occurrences is observed in offshore areas. From 1200–1600 LT, enhanced activities over coastal ocean areas are observed, which seem to lead to the increase over land. Although the diurnal variation of occurrence is very small over remote oceans, some increase is observed, such as over the ITCZ during 0000–0004 LT and 1200–1600 LT. We do not observe any particular inconsistencies between the diurnal features above and the results by Nitta and Sekine (1994), although their study focused on the convection intensity based on IR Tb and did not consider the size and evolution of the systems. Moreover, the present results are consistent with the results by Nesbitt and Zipser (2003) for MCS and the precipitation feature with ice scattering, and those by Hirose and Nakamura (2005).

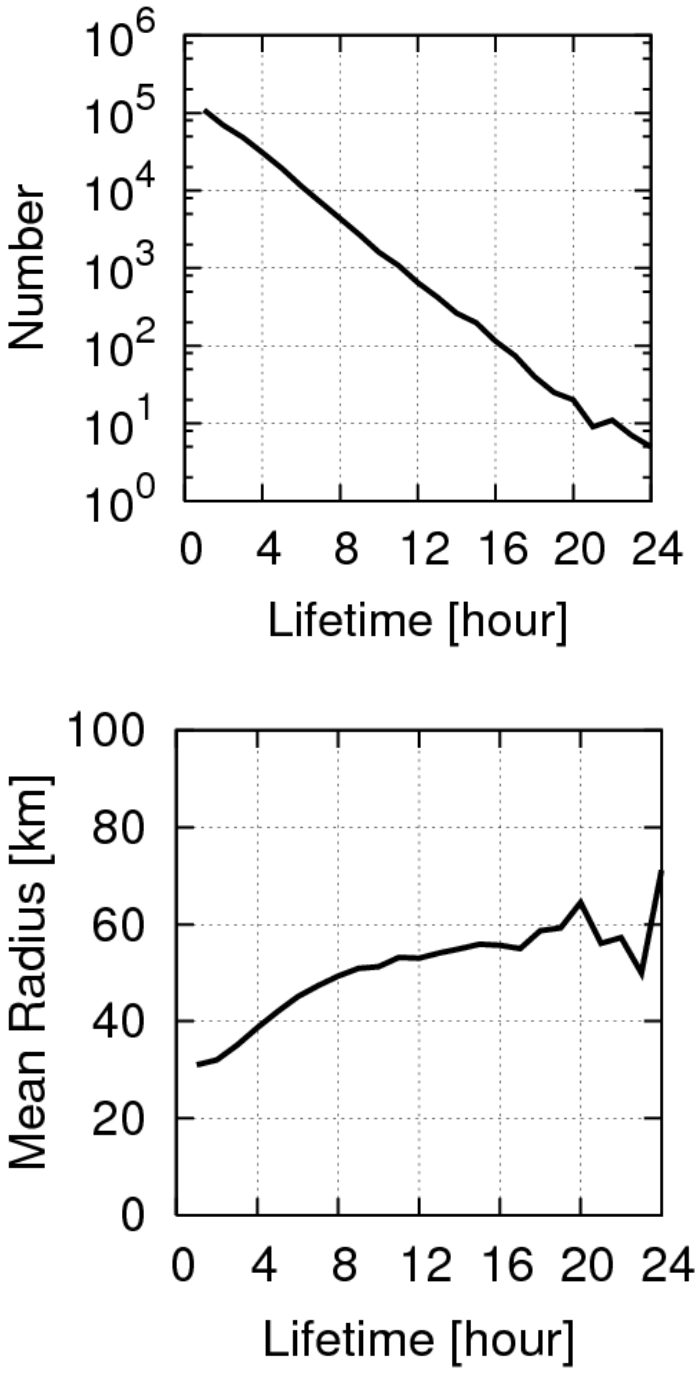

FIG. 2. Number of cold cloud systems (upper) and their mean radii (lower) during the lifetime as a function of system's lifetime during the period from June 2006 to May 2010.

(a)

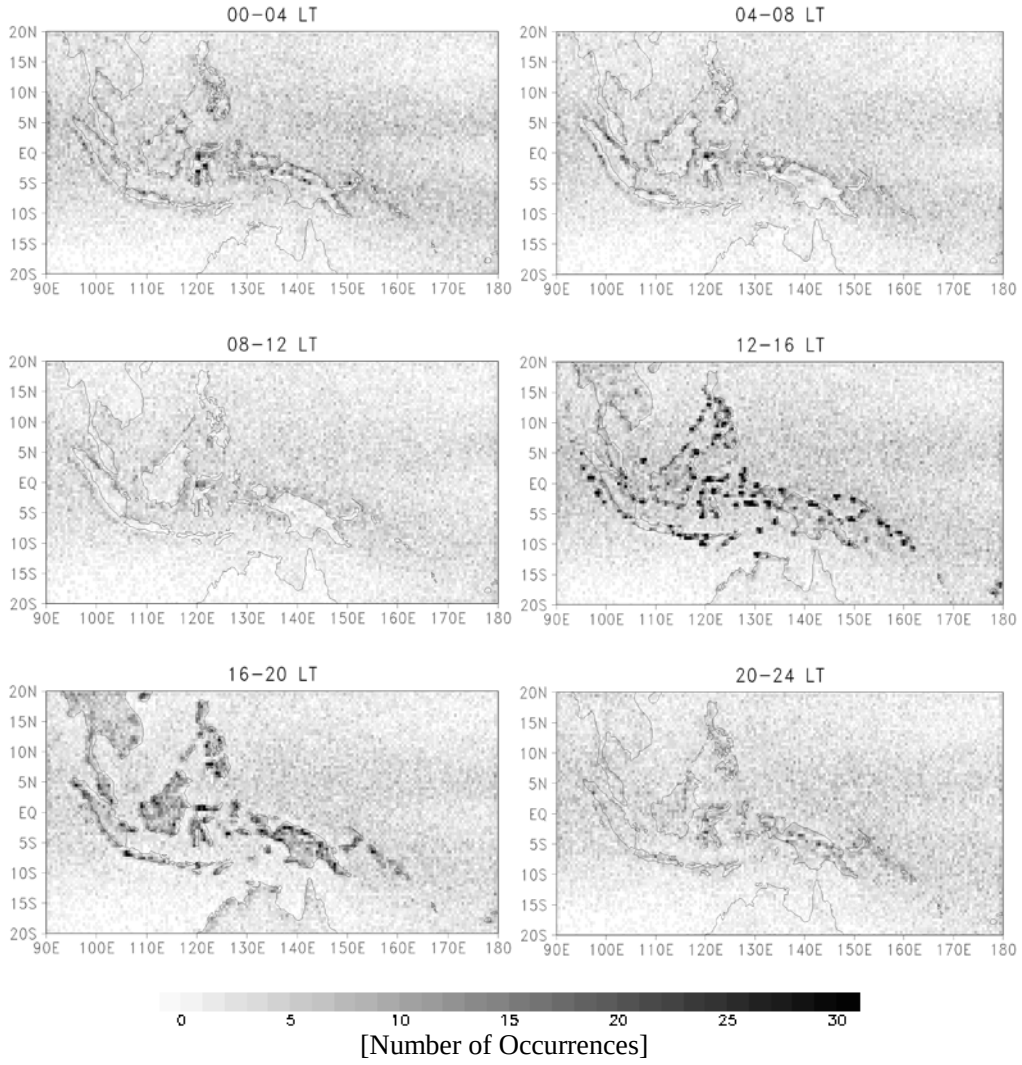

(b)

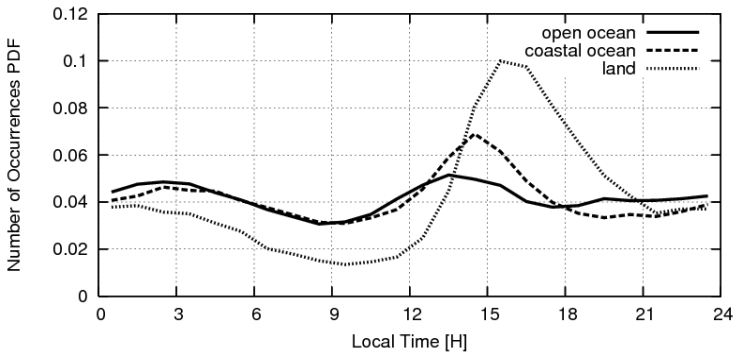

FIG. 3. (a) Geographical distributions of number of cold cloud system occurrences during the period from June 2006 to May 2010, sorted in 4 h local time bins and 0.5° resolution grids. The time of occurrence is defined by the center of lifetime. (b) PDFs of number of cold cloud system occurrences for open ocean, coastal ocean, and land areas.

3.2 Statistics of TRMM data

Two statistics, the number of cold cloud systems with TRMM synchronous observation and the ratio of the number of cold cloud systems accompanied with PR precipitation to the total number, are shown for areas over the ocean (both open and coastal ocean) and land in Figs. 4a-4b and Figs. 4c-4d, respectively. In case that any single grid of PR precipitation exists inside the cold cloud area, the system is categorized as with precipitation. Because of the difference in area between the ocean and land within our study region, the number of cold cloud systems with TRMM synchronous observations is much larger for the ocean areas. Furthermore, systems with shorter lifetimes have a large number of TRMM synchronous observations, because of the original distribution of the number of systems, as shown in Fig. 2. Despite this large number of the synchronous observation, it is evident from Figs. 4b and 4d that the ratio of the precipitation-accompanied systems is smaller for the 1 h lifetime systems than it is for the longer lifetime ones. Because of the small number of data over land as mentioned above, most of the results in this paper are presented for cases observed over the ocean. When minor differences between open ocean and coastal ocean occur, the results are averaged over both and denoted “ocean” results. In Fig. 5a, areas of cold clouds indicate changes with lifetime and elapsed time over the ocean similar to those shown by Kondo et al. (2006), indicating cloud area extension in the first half of the lifetime and reduction in the latter half. This is also consistent with the results by Machado et al. (1998), although their target lifetime range was much longer and the size threshold was much larger. Although the areas with PR precipitation seem to exhibit a similar tendency as shown in Fig. 5b, the ratio of precipitating area to cold cloud area shows a monotonic decrease with elapsed time in Fig. 5c, except for the systems with a 5 h lifetime. The systems with a 1 h lifetime have the smallest ratio of about 0.4, while others have larger values up to 0.6.

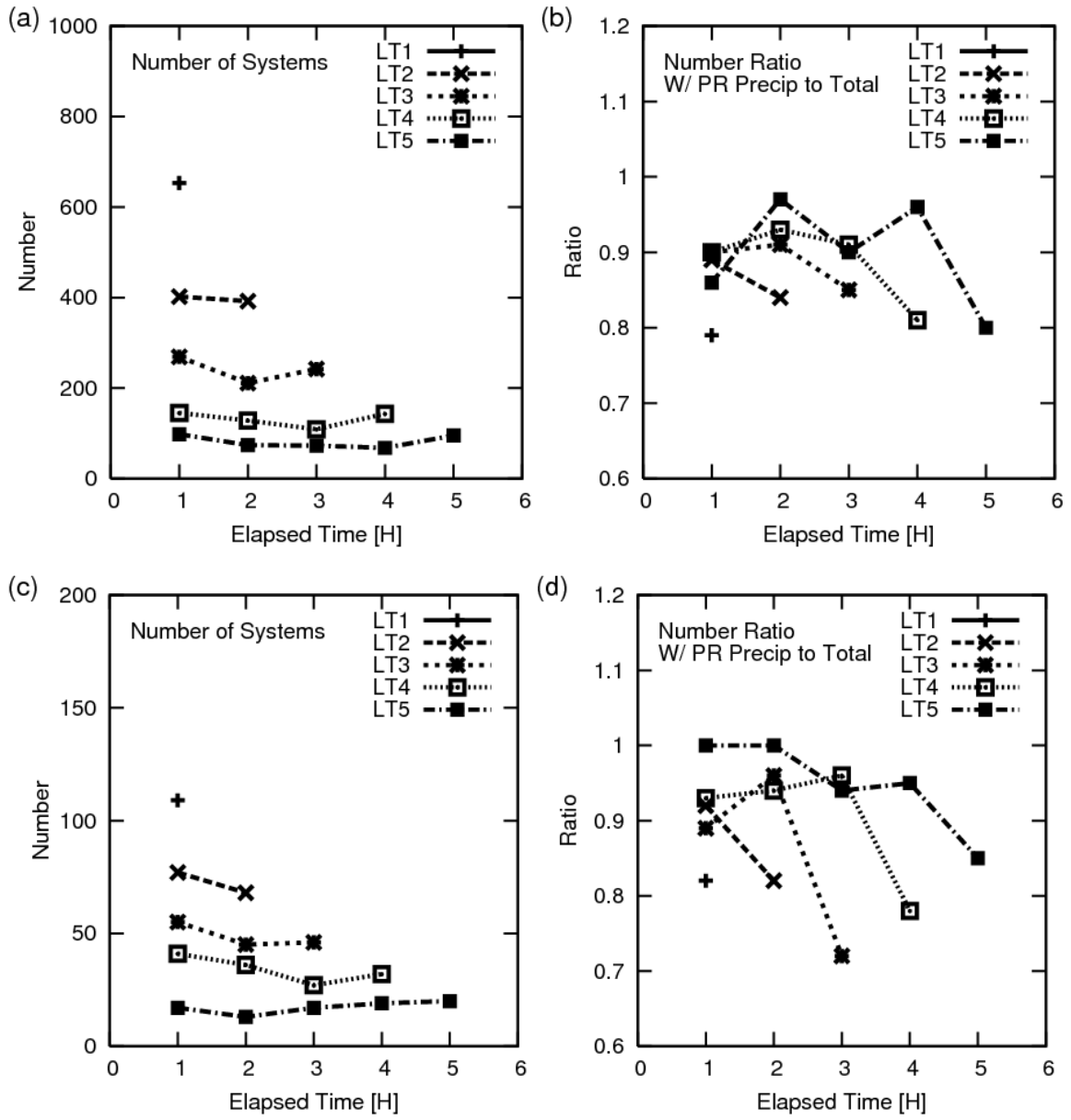

FIG. 4. Life cycle variations of (a) number of cold cloud systems synchronized with TRMM observation, and (b) ratio of cold cloud systems with PR rainfall to the total number, for 1–5 h lifetime systems over the ocean area. Panels (c) and (d) are the same plots over land area.

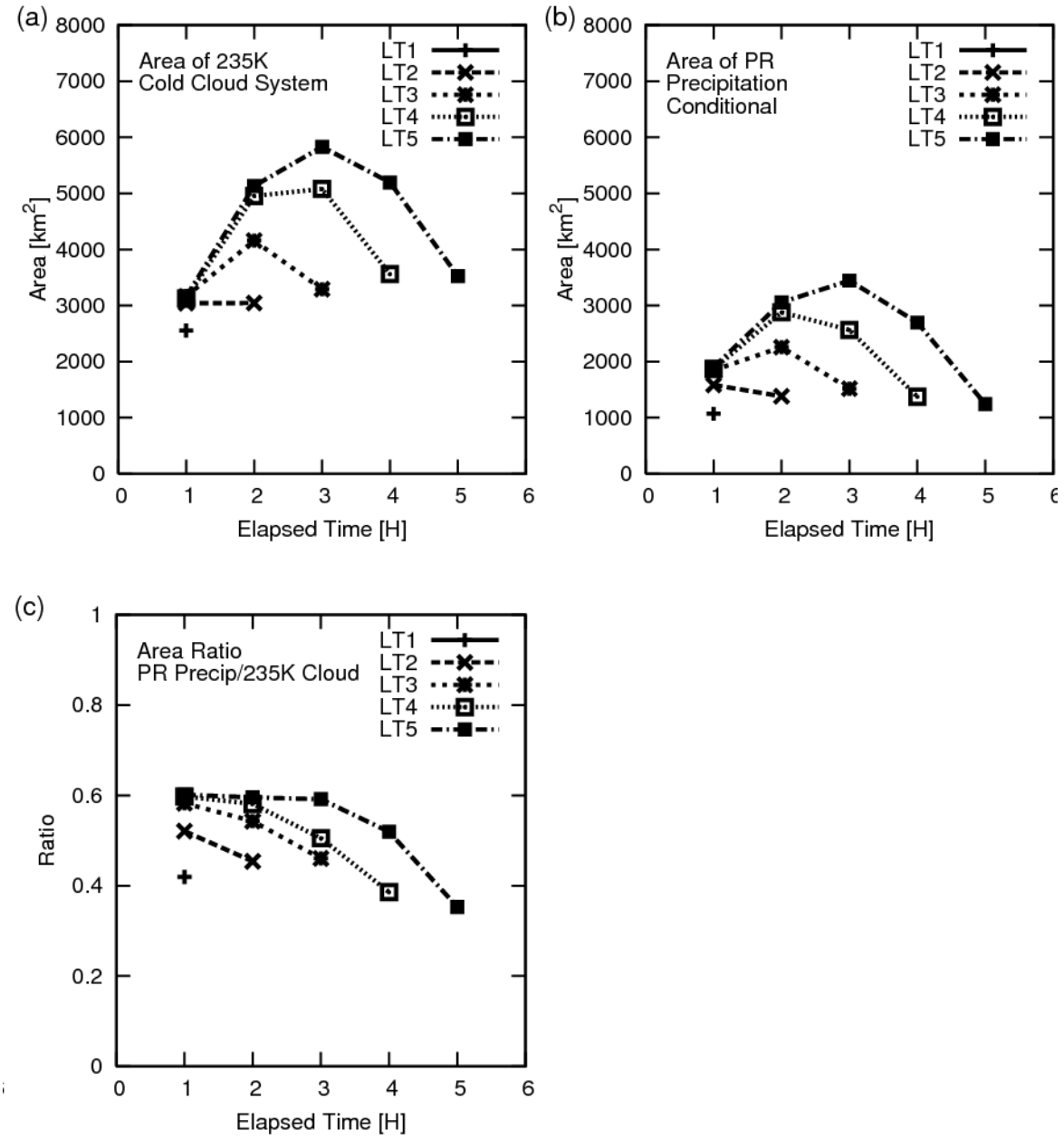

FIG. 5. Life cycle variations for 1–5 h lifetime systems (LT1-LT5) over the ocean. (a) Area of cold cloud systems, (b) area of PR rainfall within the cold cloud systems, and (c) ratio of PR rainfall area to the cold cloud area.

The average Tbs of MTSAT-1R IR1 over cold cloud areas in Fig. 6a show that systems with shorter lifetimes tend to have minimum Tb values at the beginning of the lifetime and those with longer lifetimes reach the minimum value at a later elapsed time. Statistics for the height of 25 dBZ PR reflectivity for convective rainfall in Fig. 6c show the highest value at the time of system formation and an almost monotonic decrease with elapsed time, except for 4 and 5 h lifetime systems for which the values stay constant at the 1 and 2 h elapsed time. This implies that for longer lifetime systems, precipitation top height reaches maximum values at the initial stage, while the cloud top height continues to develop in the vertical direction. The 85 GHz polarization corrected temperature (PCT85) is computed over cold cloud areas and shown in Figs. 6b. The PCT85 signature was proposed by Spencer et al. (1989) and is expressed by

$$PCT85 = 1.818 \times T_{b\_85V} - 0.818 \times T_{b\_85H}, \quad (2)$$

where T_{b_85V} and T_{b_85H} are the Tbs of the 85 GHz vertical and horizontal polarization channels, respectively. The depression of PCT85 typically originates from the scattering by large ice particles associated with precipitation and is often used for estimating rainfall over land, where the emission signature of precipitation at lower frequencies are difficult to use. The lifetime changes of PCT85 seem to be similar to those of IR Tbs in Fig. 6a. Systems with shorter lifetimes tend to have minimum values at the beginning of the lifetime and those with 5 h lifetime reach the minimum at 2 h elapsed time.

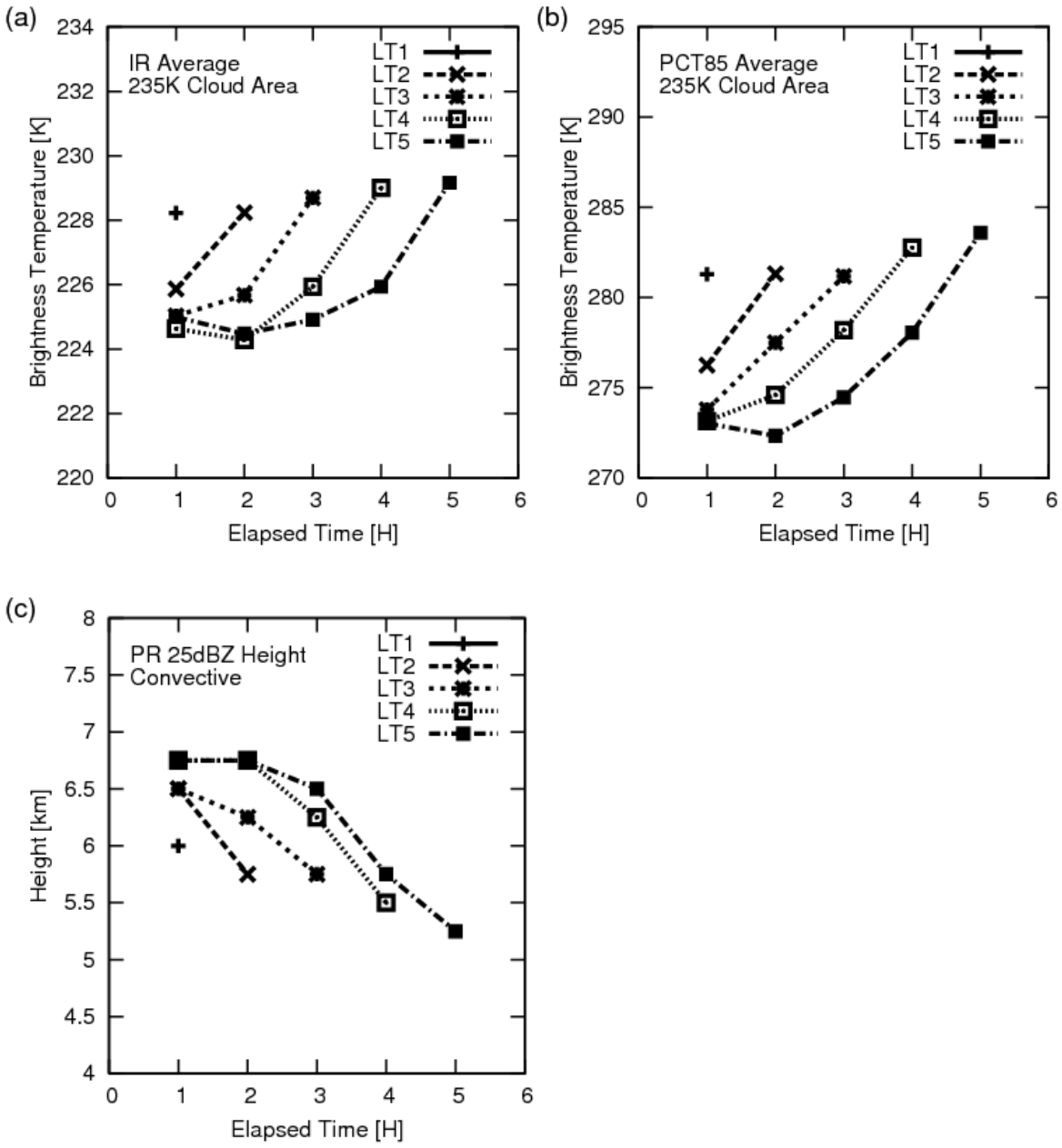

FIG. 6. Life cycle variations for 1–5 h lifetime systems (LT1-LT5) over the ocean. (a) Average IR Tb over cold cloud area, (b) average PCT85 over cold cloud area, and (c) height with PR reflectivity of 25 dBZ for convective rainfall.

Estimates of the surface rain rate are compared in Fig. 7 for TMI and PR over the ocean and land. Figures 7a and 7b show the average rain rate only over the rainfall area (conditional average rain rate) within a system over ocean for TMI and PR, respectively. Error values attached indicate 95% statistical confidence of average values with an assumption of normal distribution of samples. Figure 7c shows the ratio of the TMI conditional average rain rate to that of PR over ocean. Although both TMI and PR conditional average rain rates seem to decrease almost monotonically with elapsed time, the ratio in Fig. 7c shows some differences. For the longer lifetime systems, the ratio is slightly less than 1.0 at the time of system formation, increases above 1.0 at the later elapsed time, and then again decreases. On average during the lifetime, the ratios are close to unity for all lifetime systems. The same statistics are shown in Figs. 7d, 7e, and 7f for land areas. Although the estimated errors are larger than those over ocean due to the smaller number of data, similar tendencies in lifetime changes are observed. The values of ratio in Fig. 7f, however, indicate that the TMI conditional average rain rates significantly higher than those of PR over land about 40 to 50% on average during the lifetime.

The PR conditional rain rates averaged only over the convective rainfall area retain much higher values over the ocean as shown in Fig. 8a. In contrast to the monotonic decrease seen in Fig. 7b, the convective-conditional average rain rate peaks at the elapsed time of 2 h for the 5 h lifetime systems. The values of the conditional rain rates averaged over the stratiform rainfall area are about one-fifth to those of the convective ones, as shown in Fig. 8b in the form of a ratio. This ratio maintains an almost constant value throughout the elapsed time. The delayed peak seen in the convective-conditional average rain rates for 5 h lifetime systems is not observed in the stratiform-conditional average rain rates (not shown). The ratio of the number of convective profiles to total shown in Fig. 8c is about 0.3–0.4 at the time of

system formation and shows a monotonic decrease with elapsed time. Compared to other parameters, the two ratios in Fig. 8 show fairly similar values for different lifetime systems.

The numbers of cold cloud systems accompanied by lightning flashes detected by LIS over open ocean, coastal ocean, and land are shown in Figs. 9a, 9b, and 9c, respectively, in the form of a ratio with respect to the total number. It is clearly seen that the ratio is highest for the systems over land, lowest over open ocean, and in between the two over coastal ocean. Although it is not quite clear over open ocean, some common characteristics are observed for all surface types. In general, longer lifetime systems have higher lightning ratios. Shorter lifetime systems tend to peak at the beginning of the lifetime and longer lifetime systems' peak appear at a 1 h delay. Mattos and Machado (2011) analyzed some physical and microphysical properties of MCSs and cloud-to-ground lightning over land and coastal areas, by using the information from satellites and the Brazilian lightning detection network. They indicated that the maximum lightning frequency occurred during the growth phase close to maturation, while the average lightning density maximum was attained during the first life cycle stages. The feature in the lightning frequency is qualitatively consistent with the tendency over land in Fig. 9c, although two results differ in their definition. Regarding the areas of the lightning flashes and the average lightning flash rate per minute (neither of them shown in the figure), the differences between those over land and open ocean are a factor of 2–3, while the differences for the ratio reach a factor of about 7. In other words, substantial portion of the land-ocean differences originates from the frequency of occurrence of lightning-accompanied systems, rather than the flash rate or flash area of the systems. Boccippio et al. (2000) found from the analysis of LIS and the Optical Transient Detector (OTD) that the bulk of the order-of-magnitude differences between land and ocean regional flash rates are accounted for by differences in storm (accompanied by lightning) frequency of

occurrence, rather than differences in storm instantaneous flash rates, which only vary by a factor of 2 on average. Their findings are consistent with the present results.

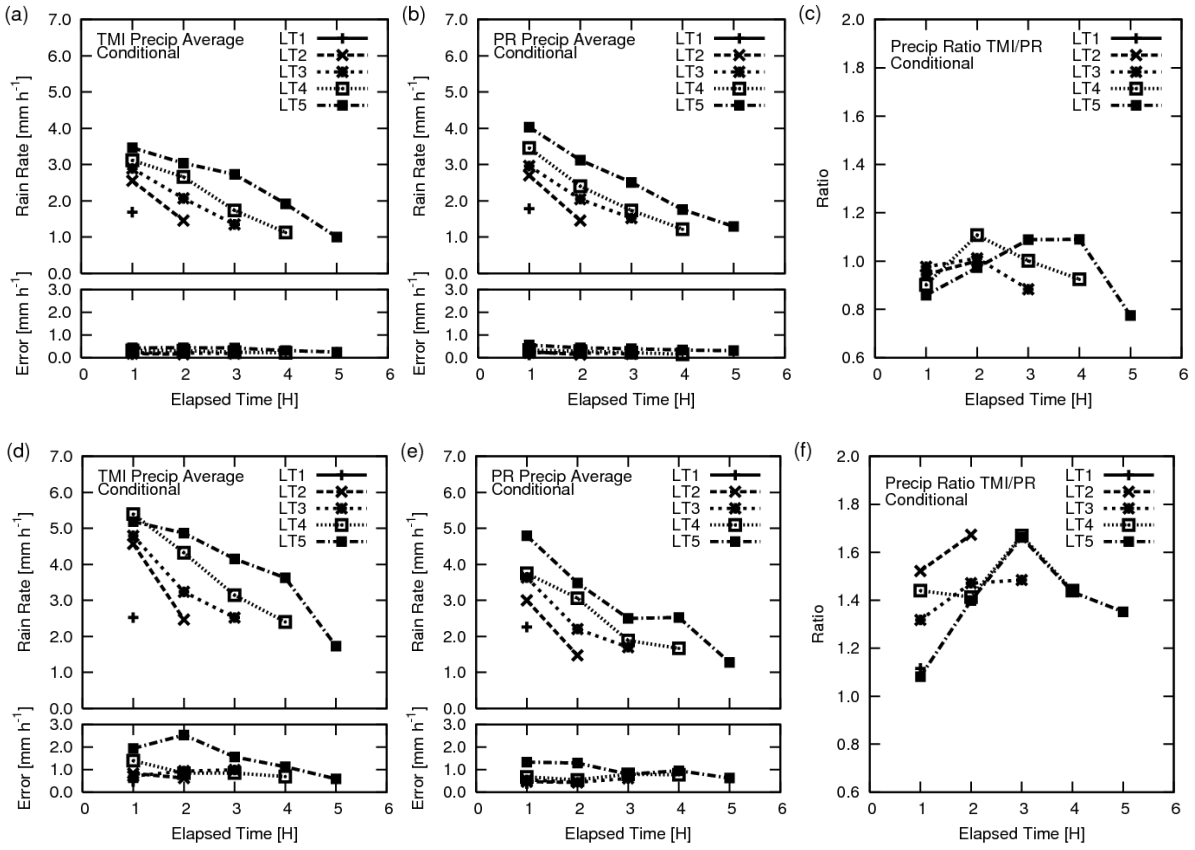

FIG. 7. Life cycle variations for 1–5 h lifetime systems over the ocean of (a) TMI surface rain rate conditionally averaged over TMI rainfall area, (b) PR near-surface rain rate conditionally averaged over PR rain area, and (c) ratio of TMI conditional rain rate to PR conditional rain rate. Panels (d), (e), and (f) are the same plots over land. Errors indicate 95% statistical confidence of average values of conditional rain rates.

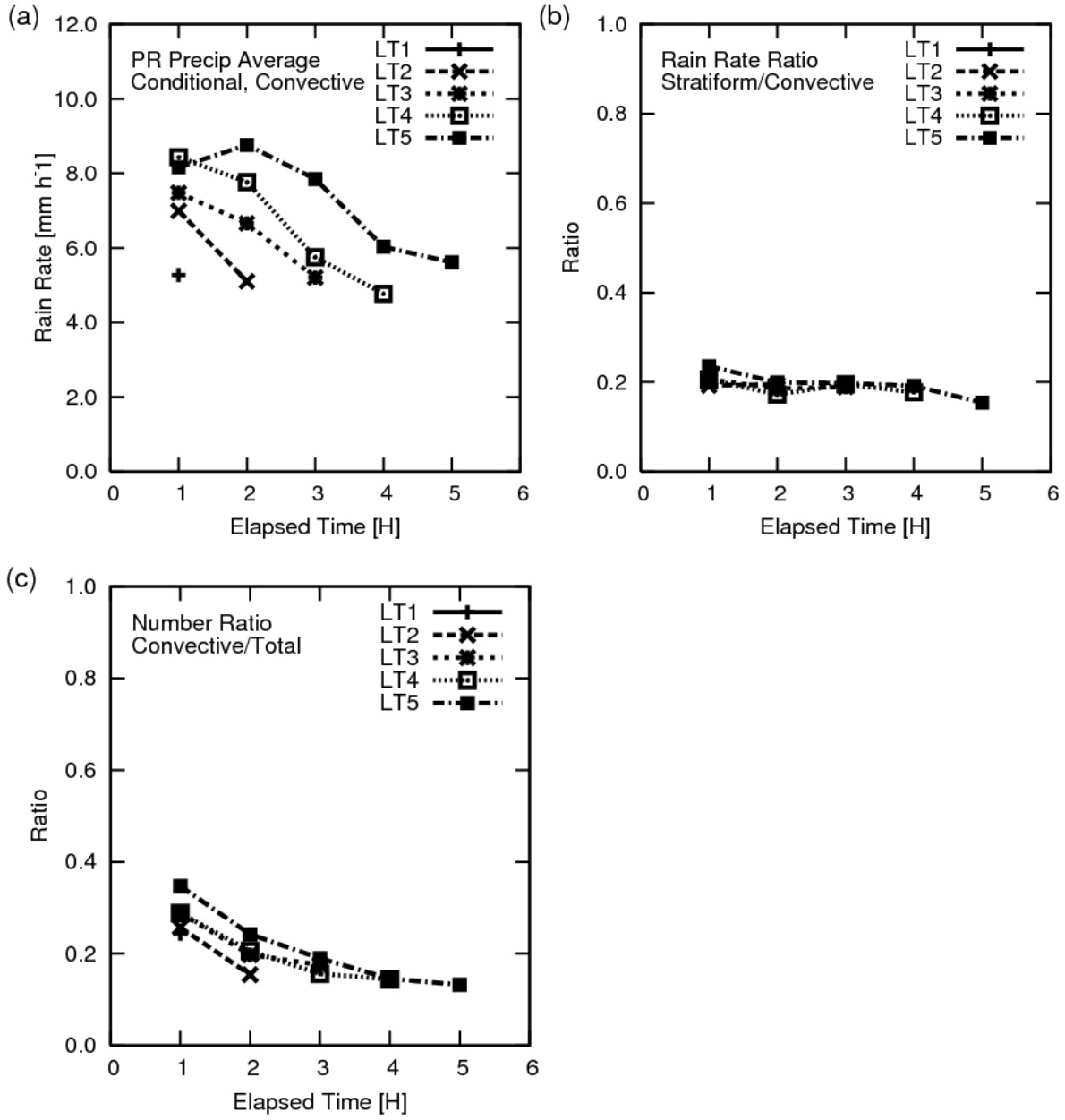

FIG. 8. Life cycle variations for 1–5 h lifetime systems over the ocean. (a) PR near surface rain rate conditionally averaged over convective rain area, (b) rain rate ratio of stratiform to convective rain, and (c) number ratio of convective to total.

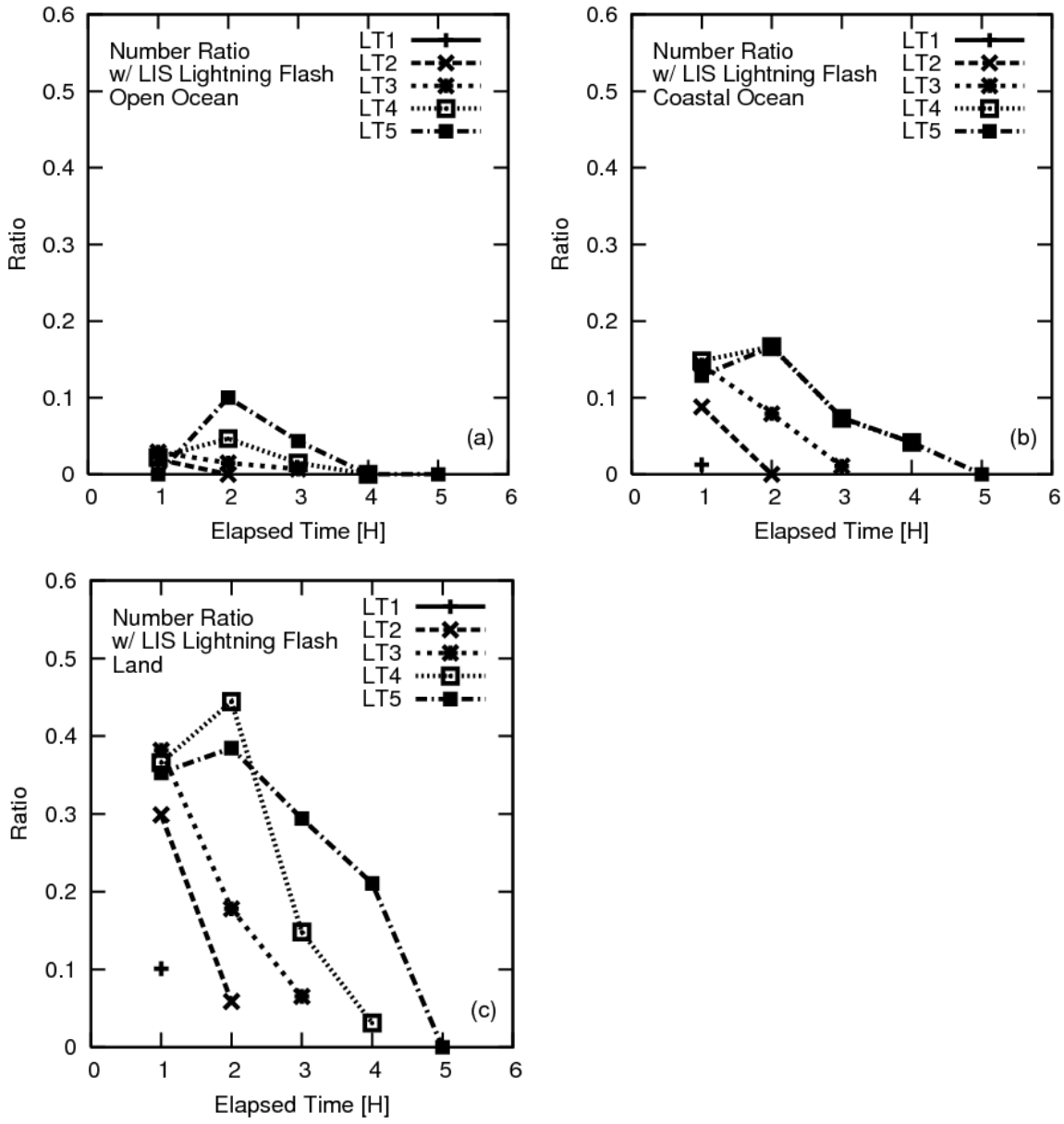

FIG. 9. Life cycle variations of the number of cold cloud systems with LIS lightning flashes in the form of ratio to the total number over (a) open ocean, (b) coastal ocean, and (c) land area for 1–5 h lifetime systems.

3.3 Statistics of PR vertical profiles

Figure 10 shows the life cycle changes of PR reflectivity over ocean areas for the 1–5 h lifetime systems, with elapsed time from 1 h to the end of lifetime. Figure 10 is expressed in the form of the two-dimensional PDFs in a reflectivity altitude plane. Only the PR reflectivity profiles with rain-certain flag are used in creating these PDFs. Since the identified cold cloud systems using the cloud tracking procedure with an IR Tb threshold of 235 K may represent convective systems in the stages from the intermediate between initiate and mature to dissipating, it is reasonable, although not necessary, to assume that the systems are accompanied by rainfall and intense radar reflectivity in the early elapsed time. Such life cycle changes are shown in Fig. 10. The PDFs in the early hours of the lifetime show a relatively broad range of distribution in radar reflectivity even at high altitude, indicating that the systems still involve appreciable convective precipitation. On the other hand, those in the later hours show weighted distribution in weaker radar reflectivity and an evident increase at the altitude of 4–5 km corresponding to the bright band, which is a unique feature of stratiform-type rainfall.

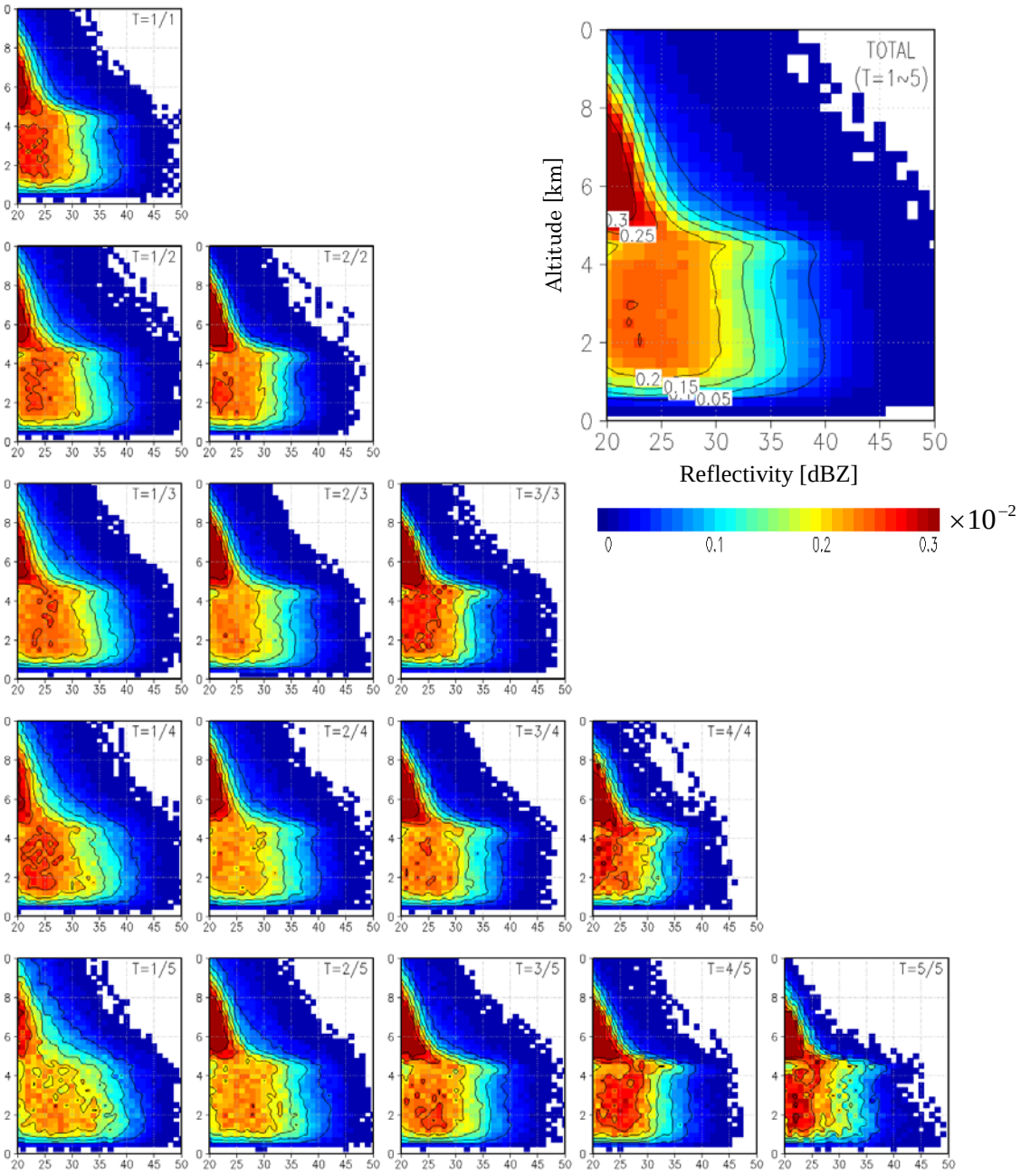

FIG. 10. Two-dimensional PDFs of PR reflectivity for 1–5 h lifetime systems. Lifetime increments from 1 to 5 h (from top to bottom) and elapsed time increments from 1 to the end of lifetime (from left to right). PDF over all lifetime systems is shown in upper right. Ordinate and abscissa of each panel are altitude [km] and radar reflectivity [dBZ], respectively.

Average PR reflectivity profiles are computed from the two-dimensional PDFs for each lifetime, elapsed time, surface type, and rain type. In computing the average reflectivity profiles, the values under the detection limit of PR (expressed by 0 dBZ in the 2A25 product) are always set to 14 dBZ. Although this is obviously not the true value, this may provide the compromise resolution since setting all the values to 0 dBZ may underestimate the average. Figure 11 shows the average profiles over ocean areas and several characteristics can be recognized. Radar reflectivity profiles at the time of system formation indicate the highest values for all lifetime systems. The longer lifetime systems tend to have larger values in the maximum reflectivity. Although some exceptions are observed, the reflectivity generally decreases with elapsed time. The profiles indicate a clear bright band feature at an altitude between 4 and 5 km. This bright band feature appears prominently in the later elapsed time for the longer lifetime systems. The characteristics of the radar reflectivity profiles shown above are consistent with the typical explanation of mature and dissipating cloud systems. Although it is self-evident from the principle of the PR rain classification algorithm explained by Awaka et al. (2009), clear differences in average reflectivity profiles are seen in Figs. 12 and 13 for convective and stratiform-type rainfall, respectively. Changes with elapsed time are most clearly seen in the reflectivity and echo height for convective systems, and in the bright band feature for the stratiform systems. The convective profiles exhibit higher reflectivity and echo height than the stratiform profiles. The 25 dBZ reflectivity height for convective rainfall in Fig. 6c is actually the intercept between the average profile in Fig. 12 and the vertical axis at 25 dBZ. The 25 dBZ reflectivity height is almost unchanged throughout the lifetime and elapsed time in the stratiform profiles. As seen in Fig. 13, at the time of system identification by 235 K threshold of IR Tbs, the bright band feature already exists and is most significant for the 1 h lifetime systems. It increases further at later elapsed time for longer lifetime systems. Figure 14 is the same graph as Fig. 11 except the rain rate

profiles over ocean areas. Profiles in the early elapsed time show an increasing tendency at the lower altitude and then become almost flat below the freezing level. This reflects the fact that the area ratio of stratiform to convective rain increases with elapsed time shown in Fig. 8c. Figure 15 shows the same panels for observations over land. Because of the insufficient number of overpass cases for the statistics as shown in Fig. 4c, the average profiles in Fig. 15 are relatively noisy compared with those over ocean areas and the changes of reflectivity values are sometimes out of sequence in elapsed time. However, we are still able to observe relative changes of the profile shape with time as seen in Fig. 11. Although the values of radar reflectivity are much higher for land profiles, relative changes such as the bright band feature do not differ much probably reflecting the fact that the area ratio of stratiform to convective rain over land is quite similar to that over ocean areas (not shown in figure). Profiles averaged over the entire lifetime and elapsed times (within the lifetime) are compared in Fig. 16 for different rain types and surface conditions. It is clearly seen that higher values and taller profiles of reflectivity and rainfall over land are solely attributed to the characteristics of the convective rainfall. Profiles of stratiform rainfall are very similar for different surface types. The land–ocean differences in the shape of the convective profiles are particularly evident for the rainfall profiles in Fig. 16e. The convective profile over land peaks at an altitude of about 3 km and those over the ocean at 1–2 km.

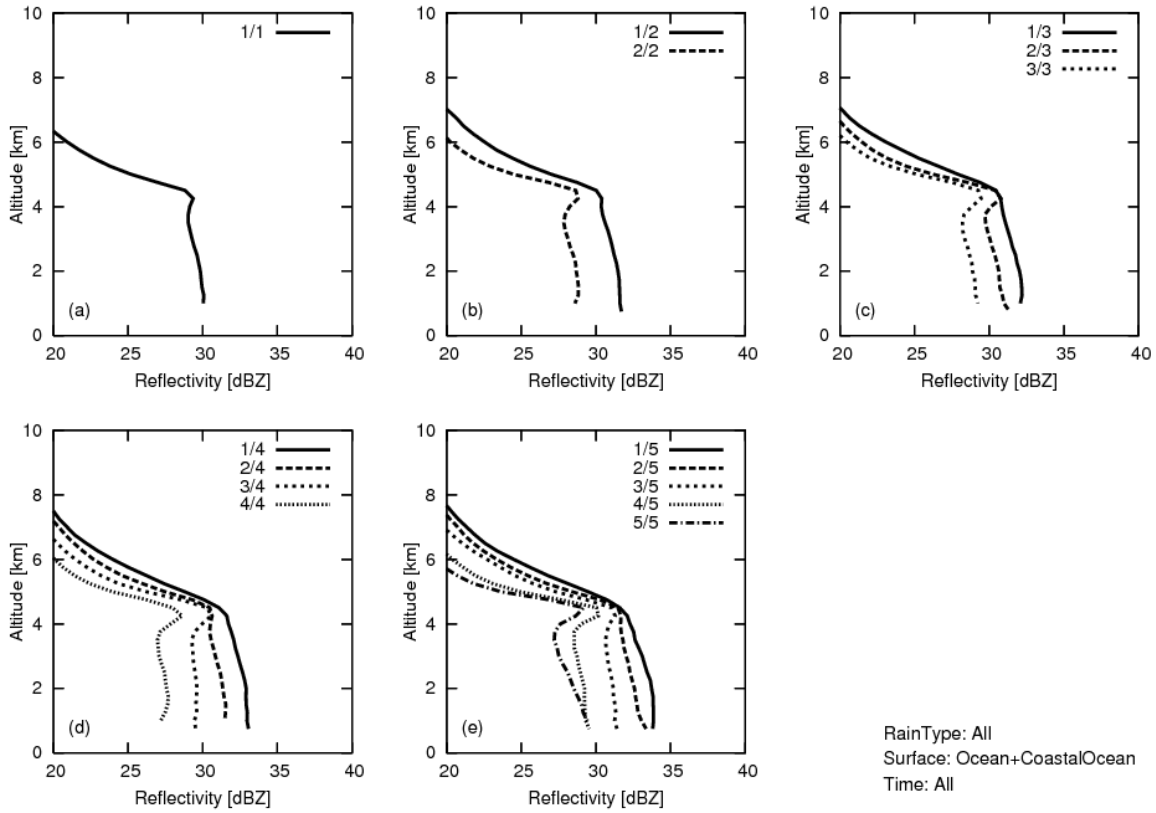

FIG. 11. Panels (a) to (e) indicate average PR reflectivity profiles of cold cloud systems with lifetimes of 1–5 h over the ocean. Different line types show elapsed time, which equals unity at the time of system formation.

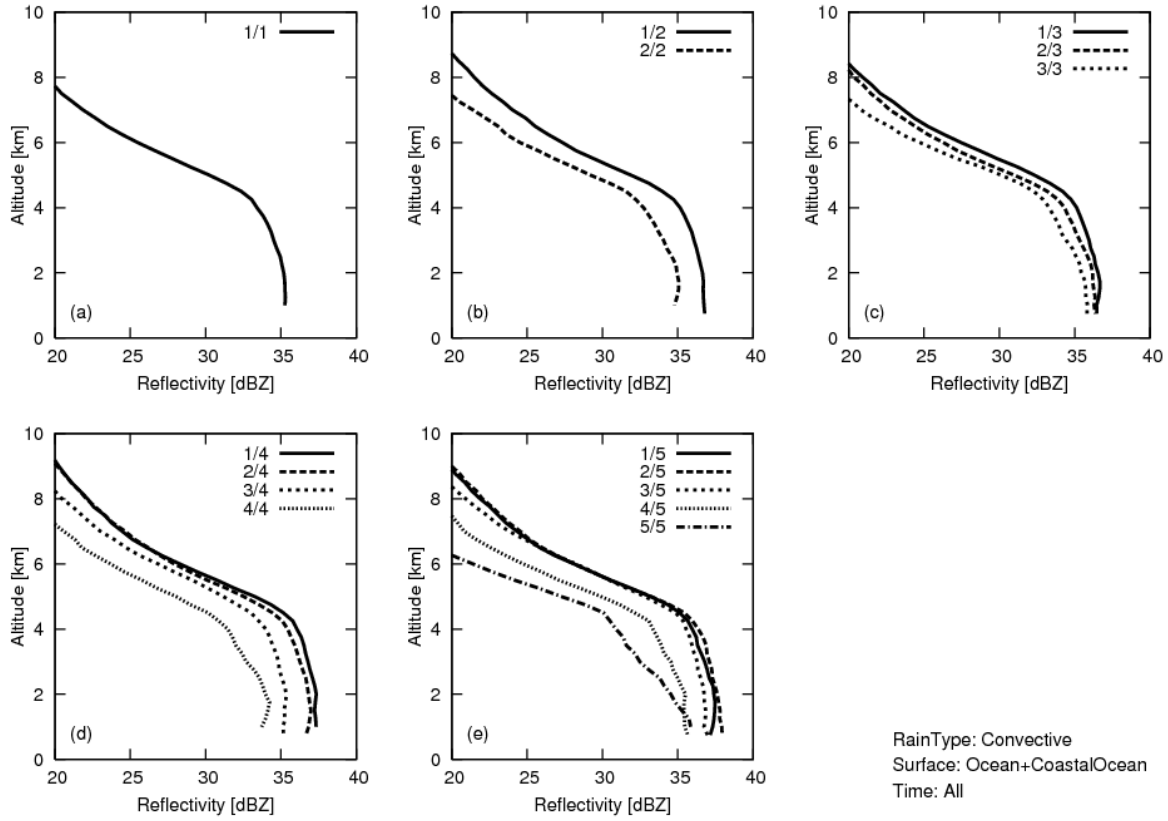

FIG. 12. Same as in Fig. 11, but for convective rain.

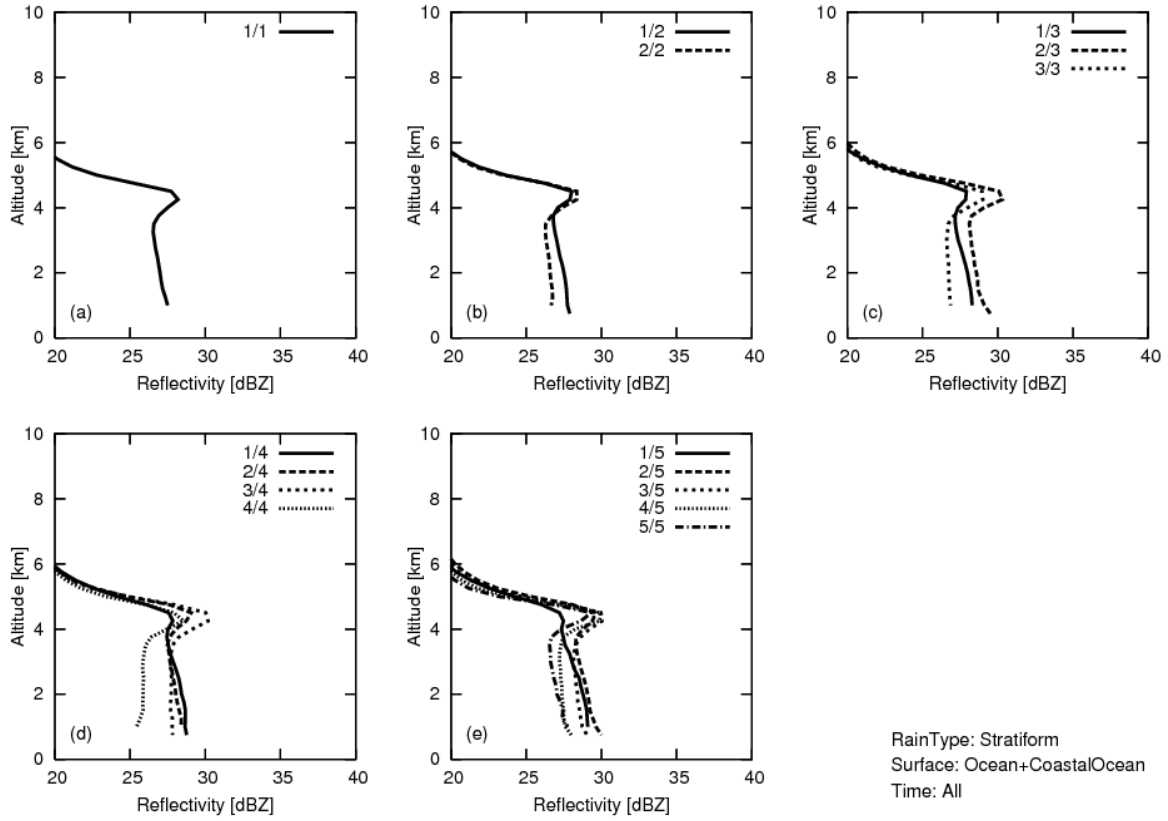

FIG. 13. Same as in Fig. 11, but for stratiform rain.

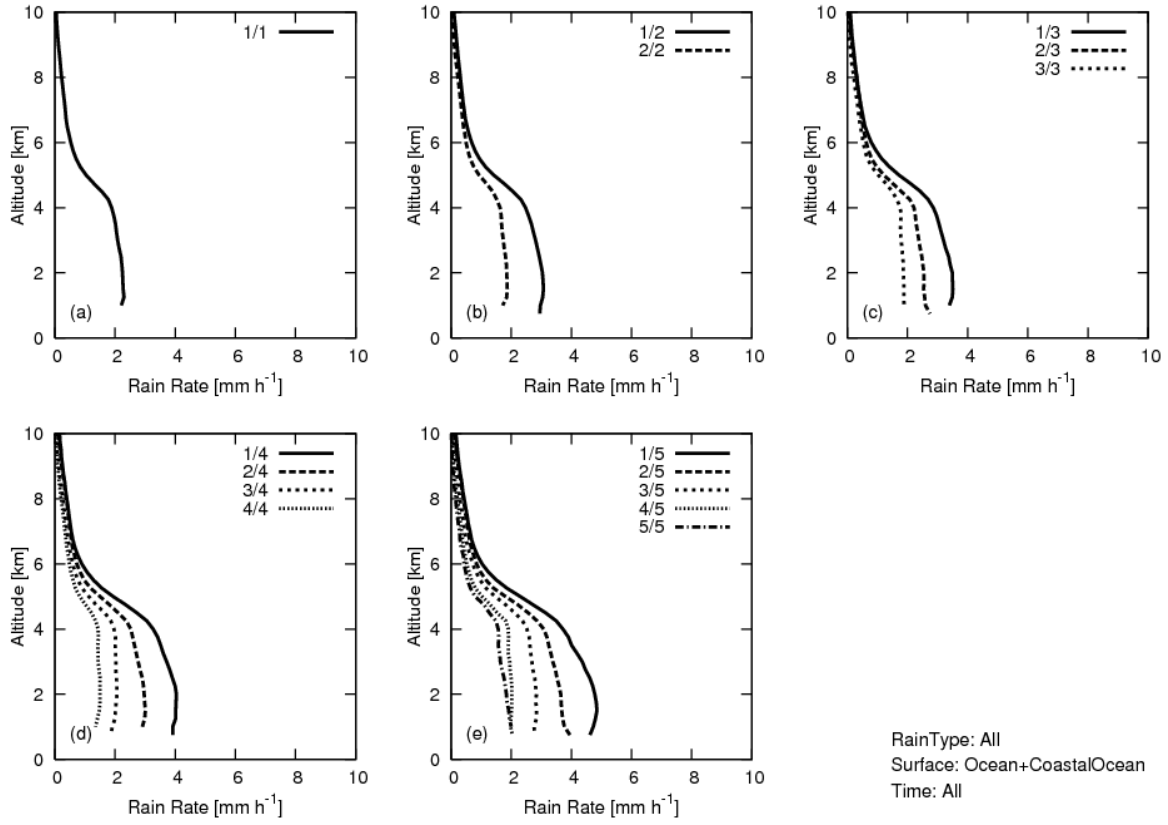

FIG. 14. Same as in Fig. 11, but for PR rain profiles.

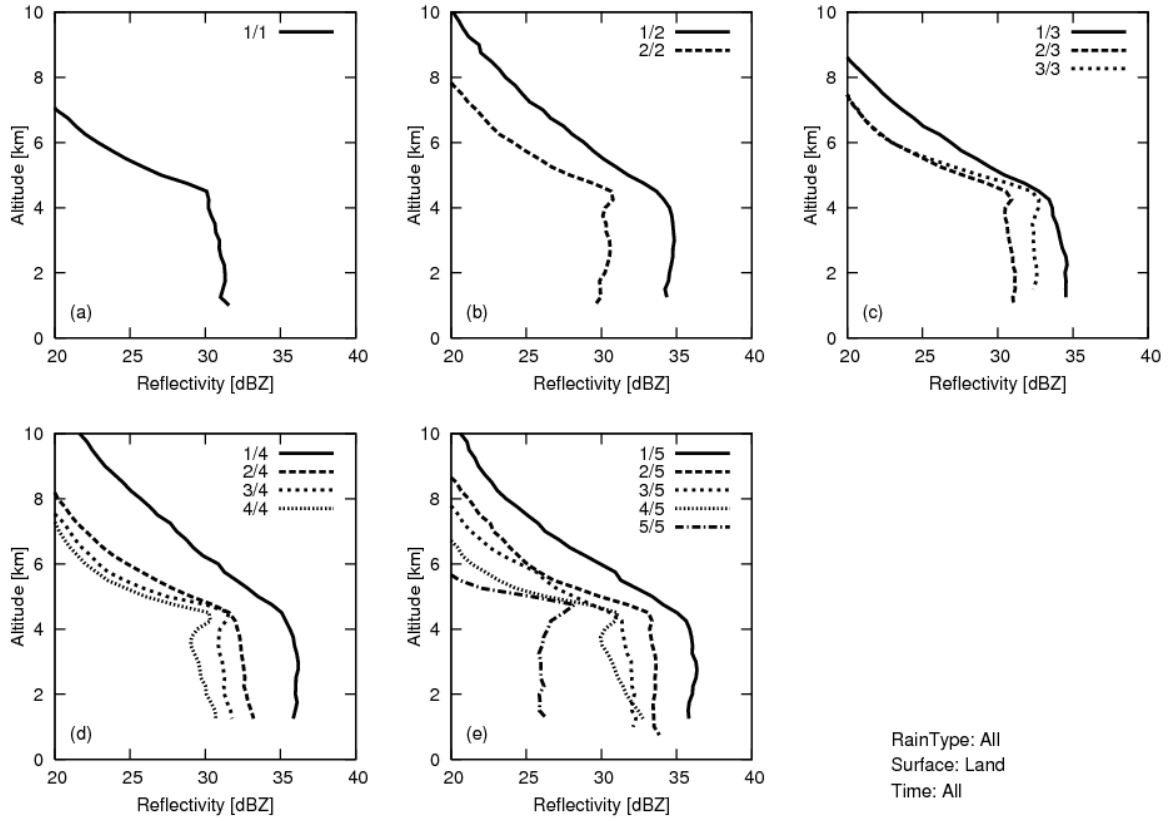

FIG. 15. Same as in Fig. 11, but for over land.

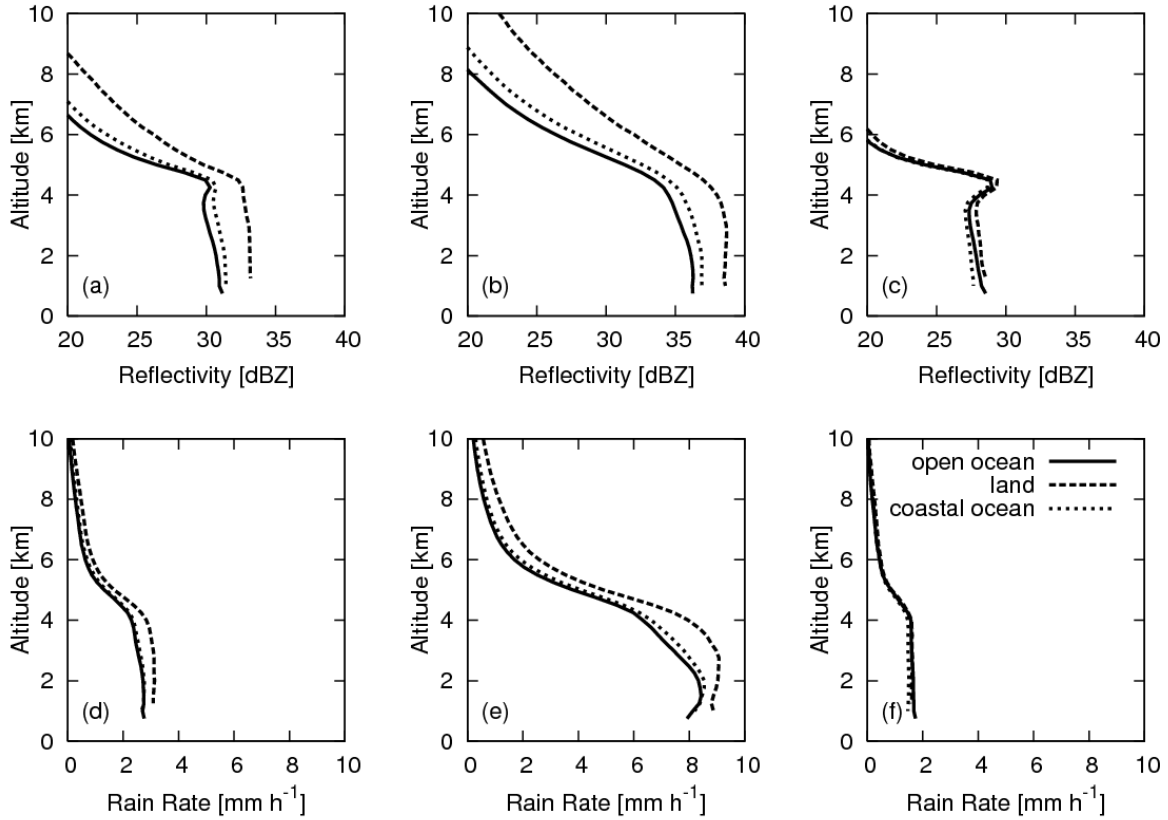

FIG. 16. Average PR reflectivity profiles (upper) and rainfall (lower) are shown for total (left), convective (middle), and stratiform (right) types of rain. Different line types indicate surface conditions.

3.4 Statistics of Q_{1R} heating profiles

Figure 17 shows life cycle variations of the areas with PR rainfall within the cold cloud systems for 1–5-lifetime systems. The convective rainfall area shown in Fig. 17 was derived by multiplying the total rainfall area shown in Fig. 5b with the ratio of the number of convective profiles to the total profiles in Fig. 8c. Although the stratiform rainfall areas in Fig. 17 actually included areas of all types of rainfall other than convective, contributions from the rainfall systems such as warm rain were negligible because the present analysis can detect only cold cloud systems. Figures 18a and 18b show the total, convective, and stratiform Q_{1R} heating profiles averaged from June 2006 to May 2010 over the entire target area and over the identified cold cloud systems with 1–5 h lifetimes. Averaging was performed over only the rainfall area (rain-conditional average). The convective heating profile in Fig. 18a indicates heating at all levels with two heating peaks at approximately 2 and 4.5 km. In contrast, the stratiform heating profile in Fig. 18a shows cooling and heating at lower and upper altitudes, respectively, with the intersection with the y-axis at 5 km. Because of averaging, the total profile in Fig. 18a shows heating at all levels with two maximums: one occurred at approximately 7.5 km mainly because of stratiform heating and other at 2 km because of convective heating. The shape of the average total heating profile in Fig. 18a was apparently affected by the large area ratio of stratiform rainfall. On the other hand, the convective heating profile in Fig. 18b shows a higher value of the peak at 4.5 km and no significant peak at 2 km. This difference is easily understood because the profiles in Fig. 18a include all types of rainfall systems and those in Fig. 18b reflect only the characteristics of isolated cold cloud systems identified by the IR Tb threshold of 235 K. The peak at 2 km in Fig. 18a possibly represents the characteristics of the cumulus congestus (Takayabu et al. 2010) and other shallow convective systems over tropical oceans.

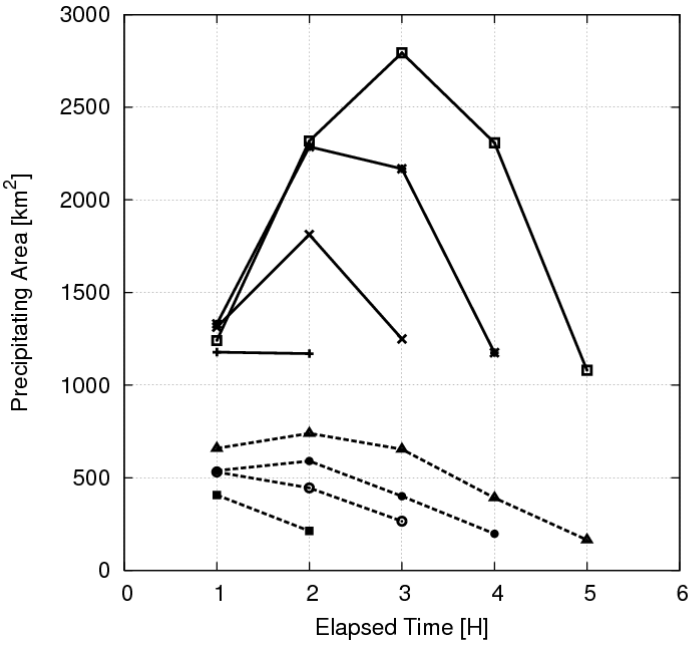

FIG. 17. Life cycle variations of PR precipitating area within cold cloud systems for 2–5 h lifetime systems over the ocean. Solid and dashed lines show the variations of areas with stratiform and convective rainfall, respectively.

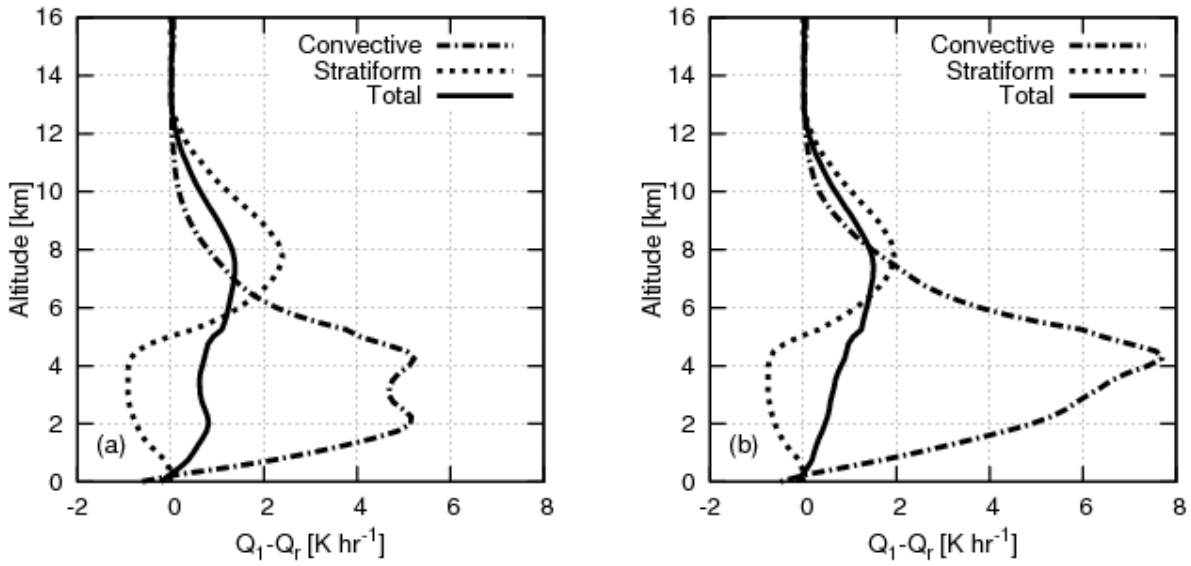

FIG. 18. Four year (June 2006–May 2010) rain-conditional average of total, convective, and stratiform Q_{1R} heating profiles over the (a) entire target areas and (b) identified cold cloud systems at 1–5 h lifetime.

Figures 19a and 19b show the geographical distribution of the rain-unconditional average Q_{1R} heating rate at 7.5 and 2 km altitudes, respectively. As discussed by Takayabu et al. (2010), lower-level heating tends to follow the distribution of sea surface temperatures, such as the belt-like distribution from the Philippine Islands to Hawaii shown in Fig. 19b. Geographical distribution of the identified cold cloud systems shown in Fig. 3a moderately resembles to that of upper-level heating. Because the shapes of stratiform heating profiles, shown in Figs. 18a and 18b, are similar, the total heating profiles in the two figures do not differ significantly in amplitude and shape, with the exception of a small peak at 2 km, shown in Fig. 18a. Therefore, regardless of the small number of occurrences and the small and short-lived characteristics of the isolated cold cloud systems observed in this study, the resulting total heating profile is similar in shape and amplitude as that over the entire tropical ocean region, which indicates that the results in this study may represent the features of heating profiles of tropical rainfall systems to some extent. The heating profiles shown in Fig. 18b are consistent with previous observational findings such as those reported by Houze (1982) and Johnson and Young (1983) for MCSs, which include upper-level warming by condensation and deposition and lower-level cooling by evaporation of raindrops and ice particle melting.

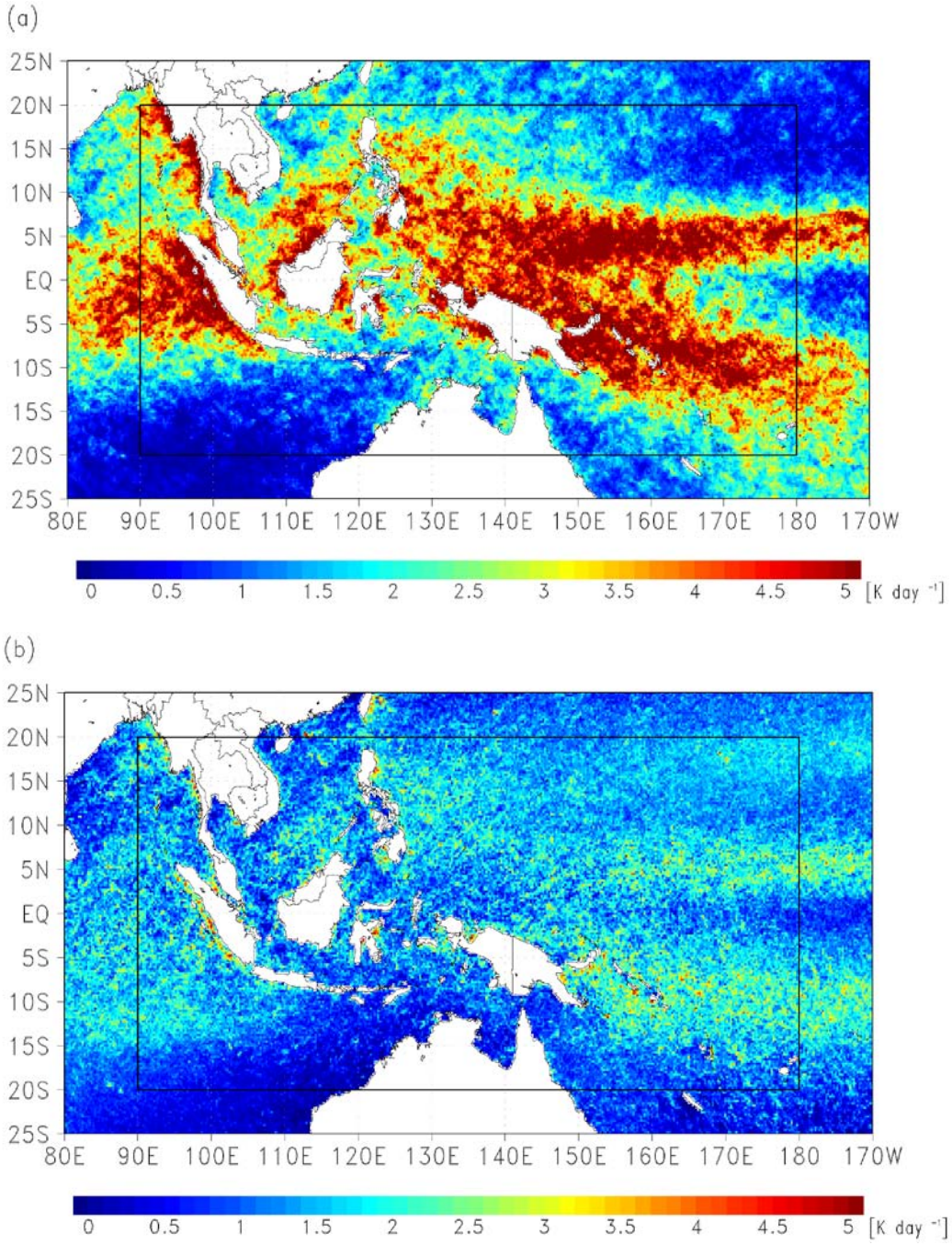

FIG. 19. Geographical distributions of four-year rain-unconditional average of Q_{1R} heating at (a) 7.5 km and (b) 2.0 km heights over tropical ocean. The black rectangular frame indicates the target area of this analysis.

Life cycle variations of convective, stratiform, and total rain-conditional average Q_{1R} heating profiles are shown in Fig. 20 for the isolated cold cloud systems. Although these profiles were obtained for all systems with 1–5 h lifetimes, only the results for the 2 h and 4 h lifetime systems are presented in the figure. For convective cases, the profiles indicate heating at all levels throughout the lifetime and clear life cycle variations, as shown in Figs. 20a and 20b for 2 h and 4 h lifetime systems, respectively. Maximum heating rates generally tended to appear at early hours of the lifetime and decreased with elapsed time. For the 4 h and 5 h lifetime systems, the heating rates at the 2 h elapsed time are comparable to those observed in the beginning. The peak altitudes near 4.5 km remained constant throughout the lifetime. The maximum heating rate was larger (smaller) for the longer lifetime systems in the beginning (end), although the difference in the beginning is not prominent, as indicated in Figs. 20a and 20b. Compared with life cycle variations of convective profiles, those in stratiform heating profiles were smaller, as shown in Figs. 20c and 20d. The heating rates in the upper troposphere slightly decreased with elapsed time, and the cooling rates at lower troposphere were nearly constant. The amplitudes and shapes of the profiles were fairly similar among 1–5 h lifetime systems, although the heating rates in the upper troposphere were rather larger in the beginning for the longer lifetime systems. The resulting total heating profiles indicate that all lifetime systems heat the atmosphere at all altitude levels throughout their lifetimes, as shown in Figs. 20e and 20f for 2 h and 4 h lifetime systems, respectively. A transition of the heating peak was observed from the middle altitude near 5 km to the upper troposphere near 8 km. The total heating profiles and their life cycle variations were considerably affected by the area ratio of convective and stratiform rainfall and its life cycle changes. The transition of the heating peak to the upper troposphere is attributed to the extension of a stratiform rainfall area in the later stages of the life cycle.

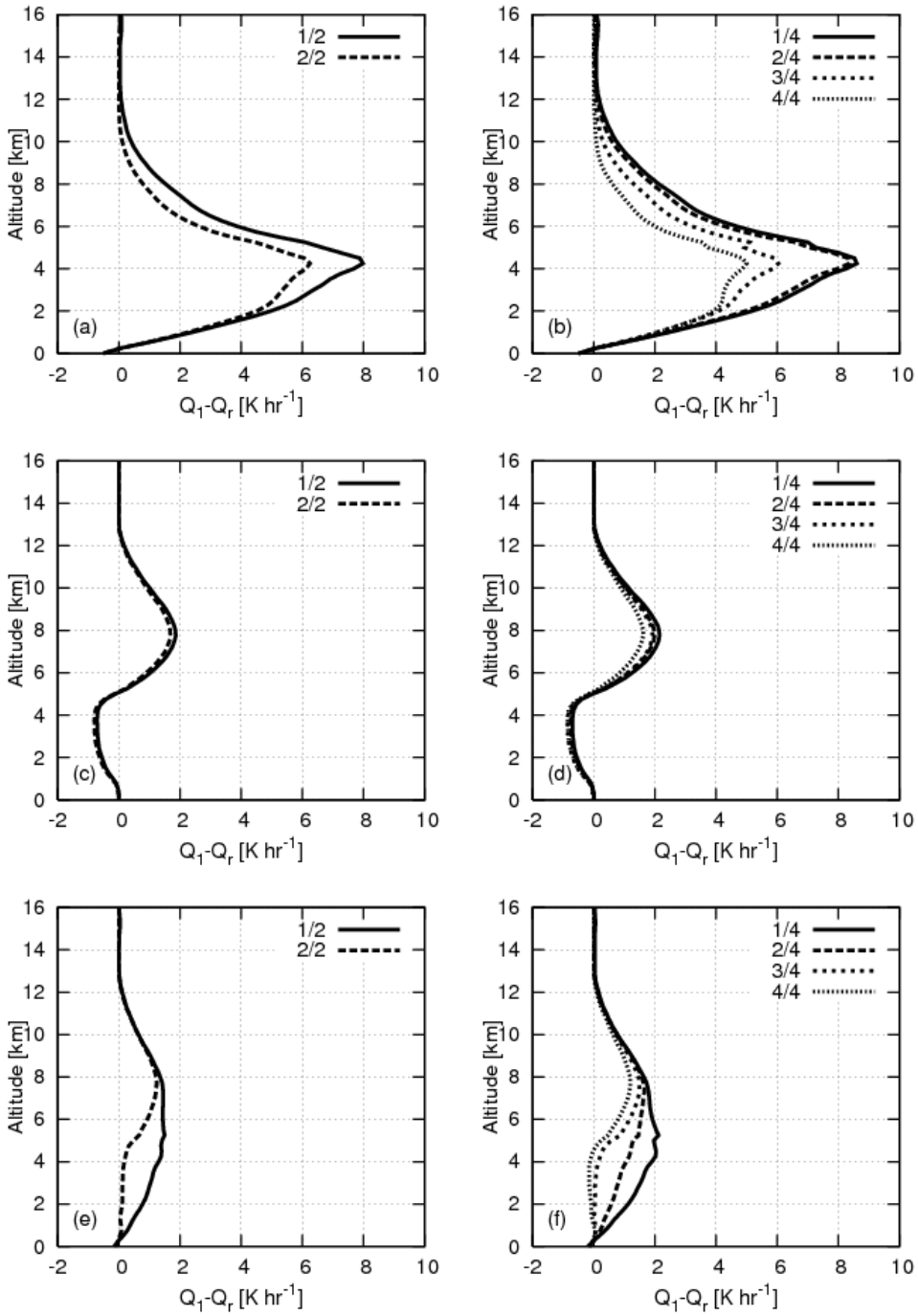

FIG. 20. Life cycle variations of convective (top), stratiform (middle), and total (bottom) Q_{1R} rain-conditional heating profiles for cold cloud systems over oceans with lifetimes of 2 h (left column) and 4 h (right column). Different line types show elapsed time, which equals unity at the time of system formation.

The total heating contribution released by a cold cloud system to the surrounding atmosphere can be expressed by the product of heating and rainfall area, as shown in Fig. 21. Because the areas of convective rainfall are larger for longer lifetime systems, as shown in Fig. 17, convective heating contributed by the 4 h lifetime system is considerably larger than that by the 2 h lifetime system in the early hours, as shown in Figs. 21a and 21b. The value is slightly smaller at the end of the lifetime because the area of the systems is comparable and the heating rate is smaller, as indicated in Figs. 17, 20a, and 20b. The differences in heating contribution between 2 h and 4 h lifetime systems are shown more clearly in Figs. 21c and 21d for stratiform profiles. Because the extension of the stratiform rainfall area is large for the 4 h lifetime system, the heating (cooling) contribution at the upper (lower) troposphere is amplified and reaches its maximum (minimum) at 2 h elapsed time. By considering the rainfall area, the maximum convective heating and stratiform heating contributions shown in Figs. 21b and 21d, respectively, are nearly comparable in amplitude for the 4 h lifetime system. Therefore, the total heating contribution by the 4 h lifetime system, shown in Fig. 21f, indicates an amplified effect of stratiform heating contribution, whereas that by the 2 h lifetime system does not differ considerably from the profiles shown in Fig. 20e.

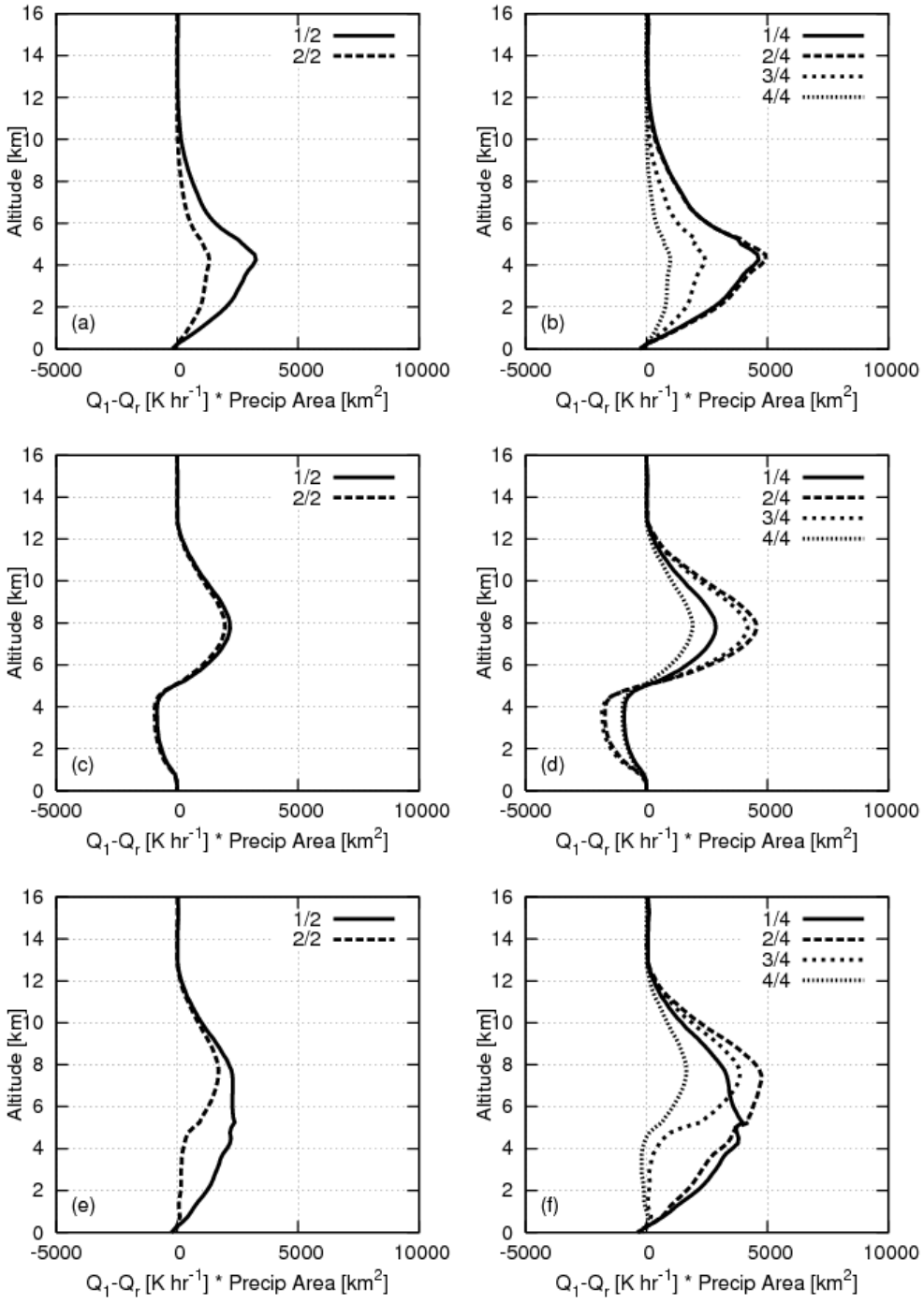

FIG. 21. Same as Fig. 20, but for with product of Q_{1R} heating and the rainfall area as abscissa.

4. Discussion

4.1 Statistical overview of life cycle for oceanic cold cloud systems

The most important results and discussion in this paper confirm the statistical but universal characteristics of the cloud's life cycle averaged over the tropics. A schematic diagram illustrating the life cycle of the tropical cold cloud systems over the ocean is shown in Fig. 22, based on the results obtained in this paper. The life cycles of 5 h and 2 h lifetime systems are shown in Figs. 22a and 22b, respectively, as examples of longer and shorter lifetime systems in this analysis.

The 5 h lifetime systems almost double their cloud area at 3 h elapsed time compared to their initial area, then decay. It is not obvious from the results in this analysis whether the cloud area actually shrinks or the IR optical depth of clouds decreases as the cloud dissipate. Although the rain area also exhibits a similar trend, the ratio of rain area to cold cloud area decreases in later elapsed times. The systems are already accompanied by considerable areas of stratiform rain from the time of system formation (indicated by the ratio of the number of convective profiles to total). This indicates that the systems are already in the intermediate stage between initial and mature stages of evolution. The average rain rate peaks at the time of system formation and decreases with elapsed time. This rain rate trend is created by the mixing of strong but small area convective rain and weaker but wide area stratiform rain. The convective-conditional average rain rate indicate the peak at the elapsed time of 2 h. The ratio of stratiform rain rate to that of convective rain maintains a fairly constant value throughout the life cycle. From the changes of PCT85, it is considered that the precipitation-size ice particles prefer the conditions in the early elapsed time and are almost synchronized with the depression of IR Tb and the convective-conditional average rain rate. Although it is not so

clear over the ocean, the frequency of lightning flashes also tends to synchronize with PCT85. As mentioned before, the 5 h lifetime systems in this study are somewhat smaller than the typical MCSs in many studies. However, the behavior of the systems appears very similar to those of MCSs, which were comprehensively reviewed by Houze (2004).

Regarding the 2 h lifetime systems, most of the parameters are somewhat smaller than those of the 5 h lifetime systems at the time of system formation, and the cloud and rain areas do not expand further at the elapsed time of 2 h. In Figs. 8c and 13, we can observe that the ratio of the stratiform rainfall area is higher and the bright band feature is clearer for the shorter lifetime systems. When compared in reverse order of time from the ending point, variations of rainfall-related parameters with elapsed time for different lifetime systems are not much different in most of the figures, except of the area information in Figs. 5a and 5b. One possible explanation of these facts is that the detection of the 2 h lifetime systems only becomes possible at the mature phase because of the small cloud area compared to the area threshold used, and we are just observing the latter half of the life cycle. If this is the case, we may observe more intense convection before the system formation, although we are not able to confirm by the present results. The existence of an optically thin remnant of an anvil cloud cannot be directly evaluated by the present analysis.

Unfortunately, the results in this study do not directly provide the reasons for the difference of the lifetime. Futyan and Del Genio (2007) performed similar analysis using the observations from the geostationary Meteosat-8 satellite and TRMM over the tropical African and neighboring Atlantic regions. They obtained similar profiles of radar reflectivity for convective cells during the mature stages of both small and larger deep convective systems, and suggested that the depth of convection does not directly control the horizontal extent of the system, while the system parameters are correlated with the convection intensity to some extent. It is generally thought that the existence of wind shear is essential to maintain the

development of cloud systems into MCS scale through sequential development of convective cells. Although it is beyond the scope of this paper, further studies considering the geographical and environmental differences will be required in the near future.

(a)

Elapsed Time	1	2	3	4	5
Cloud area [km^2]	3,200	5,100	5,800	5,200	3,500
Rain area [km^2]	1,900	3,100	3,400	2,700	1,200
Area ratio: Rain/Cloud	0.60	0.60	0.59	0.52	0.35
Number ratio: Conv./Total	0.35	0.24	0.19	0.14	0.13
Conv. 25dBZ height [km]	6.8	6.8	6.5	5.8	5.3
Cond. rain rate [mm h^{-1}]	4.0	→			1.3
Rain rate ratio: Strat./Conv.	~0.2				

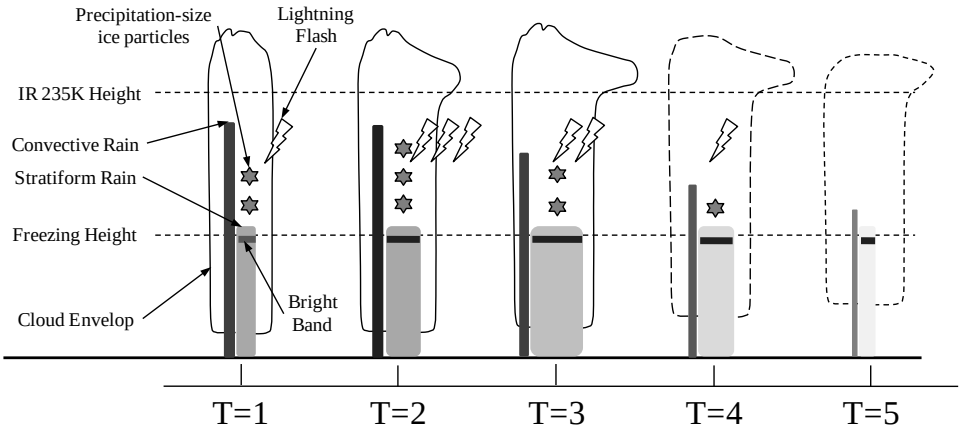

(b)

Elapsed Time	1	2
Cloud area [km^2]	3,000	3,000
Rain area [km^2]	1,600	1,400
Area ratio: Rain/Cloud	0.52	0.45
Number ratio: Conv./Total	0.26	0.15
Conv. 25dBZ height [km]	6.5	5.8
Cond. rain rate [mm h^{-1}]	2.7	1.5
Rain rate ratio: Strat./Conv.	~0.2	

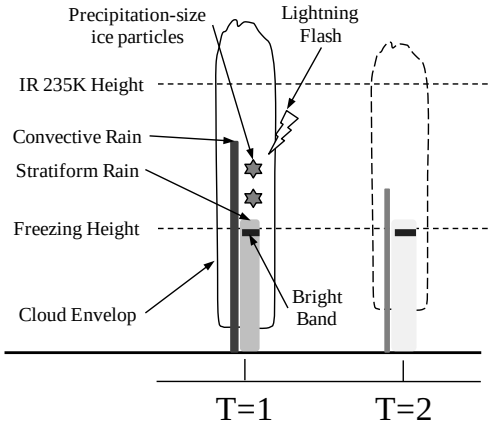

FIG. 22. Schematic diagram illustrating the life cycle of cold cloud systems over the ocean with (a) 5 h lifetime and (b) 2 h lifetime. Tables attached indicate approximate values of typical parameters based on the results of this study.

4.2 Characteristics in average PR profiles

Very clear life cycle changes of the average radar reflectivity and rain profiles are confirmed over the tropics as shown in Fig. 11. This universal view is generally consistent with the common understanding of the typical cloud life cycle. Focusing on the isolated cloud systems probably helps to obtain a clearer picture of the life cycle changes. Comparison of the average PR reflectivity profiles over the ocean and land in Figs. 11 and 15 shows larger radar echo height and time-variability for the land profiles. Although it is not shown in the figures, this is mainly attributed to the characteristics of the convective profiles. Life cycle changes of the 25 dBZ reflectivity height for convective profiles range between about 5.5 and 7 km over the ocean, and 6.5 and 10 km over land. Meanwhile, the heights of the stratiform profiles are very similar over the ocean and land, remaining nearly constant with elapsed time at an altitude of about 5 km. Futyan and Del Genio (2007) showed the median convective profiles of PR as a function of life cycle stage for large deep land and ocean convective systems. Since there are several differences in the analysis methods (e.g., their results were sorted by “life cycle stage” determined by the system size and minimum IR Tb of the tracked systems, not by elapsed time since system formation), it is not appropriate to directly compare the two results. Even so, basic differences between land and oceanic convection, such as depth, strength, and their temporal variability, are similar in both results. Regarding the profile shape below the bright band height, oceanic profiles increase their reflectivity with decrease in altitude, while the reflectivity of the land profiles tend to remain fairly constant with altitude, as seen in Figs. 11, 15, and 16a. This tendency again originates from the characteristics of convective profiles. Since convective profiles sometimes peak at an altitude of about 3 km as seen in Fig. 16b, profiles averaged over both convective and stratiform types show a flat shape. As mentioned before, this difference is more clearly seen in the rainfall

profiles. The convective rainfall profiles over the ocean peak about 1–2 km in altitude, while those over land have a maximum of about 3 km altitude as shown in Fig. 16e. Liu and Fu (2001) investigated the mean profiles of PR rainfall over the tropical belt between 15°S and 15°N. For altitudes where the rainfall rate is maximum, differences over the ocean and land were found for deep convective profiles. The maximum value appears 2–3 km over the ocean, and about 3–4 km over land. They discussed the possibility of more severe evaporation of rain drops over land, although they could not exclude the possibility of attenuation of radar echo, even though the profiles were corrected for attenuation.

4.3 Rain rate differences between PR and TMI from the life cycle viewpoint

As explained in the previous section, the ratio of TMI conditional average rain rate to that of PR over ocean in Fig. 7c indicates some lifetime variations particularly for longer lifetime systems. By comparing Fig. 7c with the lifetime changes of cloud and rainfall areas in Figs. 5a and 5b, it can be seen that the time of the maximum ratio for 4 and 5 h lifetime systems almost synchronizes with the time when systems mature. In other words, compared to the PR conditional average rain rate, the TMI conditional average rain rate provides lower values in developing phase, higher values at mature phase, and again lower values in dissipating phase. Regarding the relationship between the cloud life cycle and the differences in rainfall estimations of different instruments, related discussions were made in several papers. Rajendran and Nakazawa (2005) identified, although for the version-5 products and the tropical oceanic domain, different life stages of tropical convection by utilizing the rainfall differences and convective percentages of PR and TMI, in conjunction with infrared Tbs from the Visible and Infrared Scanner (VIRS). They noted that PR and TMI might estimate similar rain rates at the beginning of the mature stage. However, TMI started to considerably

overestimate at the later-mature and decaying stages. They concluded that it was because of the large ice scattering effect near the cloud top and the lack of melting layer emission effect in the version-5 TMI algorithm. Although we are not able to directly compare the results because of the different algorithm versions, a similar tendency is still shown over ocean areas by using the direct information of the cloud life stage. If the relationship between TMI and PR rainfall estimates can be determined for various cloud life stages and types, corrections for TMI rainfall estimates may be possible by combining geostationary IR and TMI observations. Such an idea is beyond the scope of this work and may be examined in future studies. Although it seems that similar tendencies in lifetime variations are also seen in Fig. 7f over land, they are unclear probably because of the small number of data. More prominent feature is that the TMI conditional average rain rate significantly overestimates about 40 to 50% on average during the lifetime compared to that of PR. As is well known, land rainfall algorithms for microwave radiometers differ from those over ocean. As described in McCollum and Ferraro (2003), the 2A12 version-6 algorithm uses the empirical relationship between the 85 GHz Tb and rain rate based on the collocations of TMI and PR. Extensive efforts are being made for improving the land rainfall algorithm since it is important for not only global precipitation census but also daily operational utility. As shown in Gopalan et al. (2010), the version-6 TMI rain estimates, which are used in this study, have a global “wet” bias over land compared to the PR estimates with a value of more than 30% on a global average. In their paper, the authors reported great improvements after introducing modifications in version-7, including re-examination of the TMI-PR dataset and TMI convective/stratiform ratio. The figure in their paper indicates considerable reduction in the overestimates over the Maritime Continent. In future, it may be necessary for us to check if the TMI overestimations are resolved in the version-7 products from the life cycle viewpoint.

Similar discussions are possible for the IR estimate of rainfall such as by GPI. As explained in Arkin and Meisner (1987), GPI is calculated from the product of the mean fractional coverage of clouds colder than 235 K in a 2.5° grid box. From Figs. 5 and 7, it is observed that both the rain area ratio and conditional average rain rate decrease with elapsed time. This implies that the cold cloud area with a threshold of 235 K does not track the temporal changes of total rain volume, expressed as a product of the average rain rate and the rain area. If cloud systems at different life stages randomly appear in the average window in time and space, the resulted average values of IR estimates may correlate with the true value. However, if cloud systems at a certain life stage predominantly appear in the average window, the IR estimate may produce a biased interpretation. This may be more controversial for much longer lifetime phenomena, such as persistent anvil clouds in the afternoon hours usually seen in the diurnal cycle over the ocean. Such biases, however, may be corrected in the GPCP product by the microwave/IR calibration described by Huffman et al. (1997).

From the diurnal variation viewpoint, Yamamoto et al. (2008) revealed the time shifts of diurnal variation among the different rainfall estimates and indices from PR, TMI, and VIRS, and suggested that sensor signatures that depend on convective precipitation and cloud-system development might cause these time shifts. They discussed that PR directly detected near-surface rain from the initial to mature stages, while TMI mainly observed deep convection and detected heavy rain with solid hydrometeors in the mature stage. Although the diurnal variation of cloud systems is a phenomenon on a much longer time scale and is dominated by more organized cloud systems, the life cycles appear similar to the stages of cumulonimbus clouds, as discussed in Mapes et al. (2006). A comparison between the results of Yamamoto et al. (2008) and those of the present paper shows this similar life cycle trend from the perspective of precipitation estimate.

4.4 Total heating contribution from a cold cloud system

On the basis of the present results, it is determined that the dominant factors for determining the life cycle variation of the total heating contribution from a cold cloud system are changes in the rainfall area and ratio of the stratiform rainfall, rather than changes in the shape of convective rainfall profiles. Houze (1982, 1989) demonstrated that the vertical structure of latent heat over tropical rainfall systems can be estimated by using the relative ratios of convective and stratiform rainfall. On the basis of this concept, Schumacher et al. (2004) estimated the tropical latent heating from the PR surface rainfall and stratiform rain fraction by assuming the typical heating profiles for convective and stratiform rainfall to show that the geographical and temporal variability in the stratiform rain fraction plays an important role in shaping the structure of the large-scale tropical circulation's response to precipitating cloud systems. Although a direct comparison cannot be made because of different research subjects, the present analysis does shows similarities to the previous research. However, it should be noted that the present analysis represents the cloud life cycle from the intermediate stage, between initial and mature stages, to dissipation. In addition, regional and environmental differences in heating profiles have been reported (Shige et al. 2007). For further investigation of the entire cloud life cycle over various regions, in which the shape of heating profiles may considerably vary, particularly in convective profiles, retrieval of accurate heating profile is essential. The SLH algorithm is suitable for this purpose; the algorithm is capable of retrieving realistic heating profiles throughout the cloud life cycle, as shown by Shige et al. (2004) for the evolution of a quasi-two-day oscillation. One weak point may be that this SLH algorithm cannot capture heating associated with old convective cells without rainfall at the melting level. Such issues could be further

investigated by comparing the life cycle obtained by other instruments such as CloudSat, through which direct detection of anvil clouds is possible.

5. Summary

In this study, we analyzed four years' data of MTSAT-1R and TRMM to show the statistical view of the cloud life cycle, including the changes of vertical structure of rainfall, over the Maritime Continent and parts of the tropical western Pacific. We focused on the isolated cold cloud systems without any merging and splitting processes to obtain a clear life cycle view for the fundamental unit of the convective system. We identified temporally connected cold cloud systems by using a cloud tracking procedure, searched spatiotemporally synchronized PR, TMI, and LIS observations with the systems, and then computed various statistics.

Clear life cycle changes of the average radar reflectivity and rain profiles, which are consistent with the common understanding of the typical cloud life cycle, are confirmed over the ocean area by the statistics of the satellite observations. Life cycle changes such as those of reflectivity, radar echo height, and bright band feature are clearly observed. Focusing on the isolated cloud systems may help to obtain clearer statistics of the life cycle change. Major differences between the average profiles over the ocean and land are mostly attributed to the nature of the convective profiles, whereas the stratiform profiles show similar characteristics. Compared with the convective reflectivity profiles over the ocean, those over land show larger radar echo height and time variability. In addition, the convective rainfall profiles over land peak at a higher altitude, which is similar to the results by Liu and Fu (2001).

Typical features of the cloud life cycle are obtained and summarized for the oceanic systems. For the 5 h lifetime systems, the long-lived systems in this study, the life cycle behavior appears very similar to those of typical MCSs. The identified systems start from the intermediate phase between initial and mature stages, which is supported by the considerable stratiform rain areas at the beginning, reach the mature stage with the maximal cloud and

precipitation areas at the mid-period of the lifetime, and decay. The increase of precipitating area is mostly attributed to that of stratiform precipitation. After the mature stage, the ratio of the precipitating area to the cold cloud area decreases, implying the increase of anvil clouds. The rain rate and the radar echo height indicate their peak during the early hours, and then decrease with elapsed time. Precipitation-size ice particles and the higher ratio of lightning-accompanied systems are observed during the early elapsed time, and their peaks seem to synchronize with the peak of the convective-conditional average rain rate. The 2 h lifetime systems, short-lived systems in this analysis, exhibit weaker convective features initially and do not produce the further extension of cloud and rain areas. It is speculated that the systems are already in the mature stage when they are identified, from the observations of higher ratio of stratiform rainfall area and clearer feature of bright band than those of 5 h lifetime systems at the time of system formation.

Lifetime changes of differences between conditional average rain rates of TMI and PR are observed particularly for longer lifetime systems over ocean. Compared to the PR conditional average rain rate, that of TMI provides higher values at mature phase and lower values at developing and dissipating phases. Over land, the TMI conditional average rain rate provides significantly higher values than that of PR, as reported by some studies. Also, the cold cloud area with an IR Tb threshold of 235 K, which is the basis of the GPI technique, does not track the life cycle changes of total rain volume, probably because it mainly reflects the areas of stratiform precipitation and anvil clouds, particularly in the middle and later stage of the longer lifetime systems.

Regarding the Q_{1R} heating profiles, the similarity between the total heating profiles of the identified cold cloud systems with lifetimes of 1–5 h and those over the entire tropical ocean region indicates representativeness of this analysis to some extent, regardless of a small number of occurrences and the small and short-lived characteristics of isolated cold cloud

systems. Through the present analysis, clear life cycle variations were statistically confirmed, particularly for convective heating profiles, with heating observed at all levels throughout the lifetime, constant peak levels near 4.5 km, and a decrease in heating rates with elapsed time. On the other hand, life cycle variations were small in stratiform heating profiles, with heating observed at the upper troposphere and cooling at lower levels. The resulting total heating profiles show the heating at all levels during the lifetime and transition of the heating peak from approximately 5 to 8 km with elapsed time. Because the stratiform rainfall area and its life cycle changes are large, the total heating contribution released by a cold cloud system, which is expressed by the product of heating rate and rainfall area, is dominated by changes in the rainfall area and the ratio of the stratiform rainfall, rather than by changes in the shape of convective heating profiles.

As mentioned previously, the target of the present life cycle study is limited to the cloud systems which begin from the intermediate phase between initial and mature stages. Recent studies, however, are leading to a high requirement for understanding the initiation of convective systems, and the role of shallow convections and their heating profiles in organizing cloud systems and in producing large-scale dynamics of the atmosphere. Therefore, future studies need to explore new techniques other than utilizing cold infrared Tbs to shed light on the understanding of the pre-initial and initial stage of the cloud life cycle.

Acknowledgments

First of all, I would like to express my deepest gratitude to my adviser, Professor Kenji Nakamura, for his acceptance of the author as an adult graduate student, invaluable suggestions, and enduring encouragements for my slow-paced progress. I wish to thank Professor Hirohiko Masunaga for his various advise and elegant suggestions for my study. I also wish to thank Professor Hiroshi Ueda for his constructive comments and discussions. I also wish to thank all the members of the Laboratory of Satellite Meteorology and the Laboratory for Cloud and Precipitation Climatology, particularly Ms. Tomoko Tanaka and Ms. Fumie Akimoto Furuzawa, for their helpful discussions and overall support. Provision of the cloud tracking program, which was indispensable for this study, from Ms. Yoshimi Kawano (Kondo) is also gratefully acknowledged. This study was conducted as an adult graduate student while I continued to belong to the JAXA Earth Observation Research Center (EORC). I would like to express thank to Mr. Toru Fukuda, Director of EORC, and all the members of EORC for their understanding and support. The gridded MTSAT-1R data were processed, archived, and made available by the Center for Environmental Remote Sensing (CEReS), Chiba University. The TRMM TMI products (1B11 and 2A12) and PR products (2A25 and latent heat research product) were provided by the NASA Goddard Earth Sciences Data and Information Services Center and JAXA, respectively. The TRMM LIS Science Data were obtained from the NASA EOSDIS Global Hydrology Resource Center (GHRC) Distributed Active Archive Center (DAAC). Finally, I am grateful to my whole family. It was not possible to devote time for this study without the patience and help of my wife.

References

Adler, R. F., G. J. Huffman, A. Chang, R. Ferraro, P.-P. Xie, J. Janowiak, B. Rudolf, U. Schneider, S. Curtis, D. Bolvin, A. Gruber, J. Susskind, P. Arkin, and E. Nelkin, 2003: The version-2 Global Precipitation Climatology Project (GPCP) monthly precipitation analysis (1979-present). *J. Hydrometeor.*, **4**, 1147-1167.

Arkin, P. A., and B. N. Meisner, 1987: The relationship between large-scale convective rainfall and cold cloud over the western hemisphere during 1982-84. *Mon. Wea. Rev.*, **115**, 51-74.

Awaka, J., T. Iguchi, and K. Okamoto, 2009: TRMM PR standard algorithm 2A23 and its performance on bright band detection. *J. Meteor. Soc. Japan*, **87A**, 31-52.

Boccippio, D. J., S. J. Goodman, and S. Heckman, 2000: Regional differences in tropical lightning distributions. *J. Appl. Meteor.*, **39**, 2231-2248.

Boccippio, D. J., W. J. Koshak, and R. J. Blakeslee, 2002: Performance assessment of the Optical Transient Detector and Lightning Imaging Sensor. Part I: predicted diurnal variability. *J. Atmos. Oceanic Technol.*, **19**, 1318-1332.

Boer, E. R., and V. Ramanathan, 1997: Lagrangian approach for deriving cloud characteristics from satellite observations and its implications to cloud parameterization. *J. Geophys. Res.*, **108**, 21383-21399.

Chen, S., and R. Houze, 1997: Diurnal variation and life-cycle of deep convective systems over the tropical Pacific warm pool. *Q. J. R. Meteorol. Soc.*, **123**, 357-388.

Christian, H. J., 1999: Optical detection of lightning from space. *Proc. 11th Int. Conf. on Atmospheric Electricity*, Guntersville, AL, NASA/CP-1999-209261, 715-718.

Futyan, J. M., and A. D. Del Genio, 2007: Deep convective system evolution over Africa and the Tropical Atlantic. *J. Climate*, **20**, 5041-5060.

Gopalan, K., N.-Y. Wang, R. Ferraro, and C. Liu, 2010: Status of the TRMM 2A12 Land Precipitation Algorithm. *J. Atmos. Oceanic Technol.*, **27**, 1343-1354.

Hartmann, D. L., H. H. Hendon, and R. A. Houze Jr., 1984: Some implications of the mesoscale circulations in tropical cloud clusters for large-scale dynamics and climate. *J. Atmos. Sci.*, **41**, 113-121.

Hirose, M. and K. Nakamura, 2005: Spatial and diurnal variation of precipitation systems over Asia observed by the TRMM Precipitation Radar. *J. Geophys. Res.*, **110**, D05106, 10.1029/2004JD004815.

Houze, R. A., Jr., 1982: Cloud clusters and large-scale vertical motions in the tropics. *J. Meteor. Soc. Japan*, **60**, 396-410.

Houze, R. A., Jr., 1989: Observed structure of mesoscale convective systems and implications for large-scale heating. *Quart. J. Roy. Meteor. Soc.*, **115**, 425-461.

Houze, R.A., Jr., 1993: Cloud Dynamics. Academic Press, 573 pp.

Houze, R.A., Jr., 2004: Mesoscale convective systems. *Rev. Geophys.*, **42**, RG4003, doi:10.1029/2004RG000150.

Huffman, G. J., R. F. Adler, P. Arkin, A. Chang, R. Ferraro, A. Gruber, J. Janowiak, A. McNab, B. Rudolf, and U. Schneider, 1997: The Global Precipitation Climatology Project (GPCP) combined precipitation dataset. *Bull. Amer. Meteor. Soc.*, **78**, 5-20.

Iguchi, T., T. Kozu, J. Kwiatkowski, R. Meneghini, J. Awaka, and K. Okamoto, 2009: Uncertainties in the rain profiling algorithm for the TRMM Precipitation Radar. *J. Meteor. Soc. Japan*, **87A**, 1-30.

Inoue, T., D. Vila, K. Rajendran, A. Hamada, X. Wu, and L. A. T. Machado, 2009: Life cycle of deep convective systems over the eastern tropical Pacific observed by TRMM and GOES-W. *J. Meteor. Soc. Japan*, **87A**, 381-391.

Johnson, R. H., and G. S. Young, 1983: Heat and moisture budgets of tropical mesoscale anvil clouds. *J. Atmos. Sci.*, **40**, 2138-2147.

Kigawa, S., 2001: Overview of MTSAT-1R Imager. *Meteorological Satellite Center Technical Note*, **39**, 33-37.

Kondo, Y., A. Higuchi, and K. Nakamura, 2006: Small-scale cloud activity over the Maritime Continent and the Western Pacific as revealed by satellite data. *Mon. Wea. Rev.*, **134**, 1581-1599.

Kozu, T., T. Kawanishi, H. Kuroiwa, M. Kojima, K. Oikawa, H. Nakatsuka, and K. Nishikawa, 2001: Development of Precipitation Radar onboard the Tropical Rainfall Measuring Mission (TRMM) satellite. *IEEE Trans. Geosci. Remote Sens.*, **39**, 102-116.

Kummerow, C., W. Barnes, T. Kozu, J. Shiue, and J. Simpson, 1998: The Tropical Rainfall Measuring Mission (TRMM) Sensor Package. *J. Atmos. Oceanic Technol.*, **15**, 809-817.

Liu, G., and Y. Fu, 2001: The characteristics of tropical precipitation profiles as inferred from satellite radar measurements. *J. Meteor. Soc. Japan*, **79**, 131-143.

Machado, L. A. T., W. B. Rossow, R. L. Guedes, and A. W. Walker, 1998: Life cycle variations of mesoscale convective systems over the Americas. *Mon. Wea. Rev.*, **126**, 1630-1654.

Mapes, B. E., and R. A. Houze, 1993: Cloud clusters and superclusters over the oceanic warm pool. *Mon. Wea. Rev.*, **121**, 1398-1415.

Mapes, B., S. Tulich, J. Lin, and P. Zuidema, 2006: The mesoscale convection life cycle: Building block or prototype for large-scale tropical waves? *Dyn. Atmos. Oceans*, **42**, 3-29.

Mapes, B., R. Milliff, and J. Morzel, 2009: Composite life cycle of maritime tropical mesoscale convective systems in scatterometer and microwave satellite observations. *J. Atmos. Sci.*, **66**, 199-208.

Masunaga, H., 2012: A satellite study of the atmospheric forcing and response to moist convection over tropical and subtropical oceans. *J. Atmos. Sci.*, **69**, 150-167.

Mathon, V., and H. Laurent, 2001: Life cycle of Sahelian mesoscale convective cloud systems. *Q. J. R. Meteorol. Soc.*, **127**, 377-406.

Mattos, E. V. and L. A. T. Machado, 2011: Cloud-to-ground lightning and mesoscale convective systems. *Atmos. Res.*, **99**, 377-390.

McCollum, J., and R. Ferraro, 2003: Next generation of NOAA/NESDIS TMI, SSM/I, and AMSR-E microwave land rainfall algorithms. *J. Geophys. Res.*, **108**, 8382, doi:10.1029/2001JD001512.

Nesbitt, S. W., and E. J. Zipser, 2003: The diurnal cycle of rainfall and convective intensity according to three years of TRMM measurements. *J. Climate*, **16**, 1456-1475.

Nitta, T. and S. Sekine, 1994: Diurnal variation of convective activity over the tropical western Pacific. *J. Meteor. Soc. Japan*, **72**, 627-641.

Rajendran, K., and T. Nakazawa, 2005: Systematic differences between TRMM 3G68 PR and TMI rainfall estimates and the possible association with life cycle of convection. SOLA, **1**, 165-168.

Schumacher, C., R. A. Houze Jr., and I. Kraucunas, 2004: The tropical dynamical response to latent heating estimates derived from the TRMM precipitation radar. *J. Atmos. Sci.*, **61**, 1341-1358.

Shige, S., Y. N. Takayabu, W.-K. Tao and D. E. Johnson, 2004: Spectral retrieval of latent heating profiles from TRMM PR data. Part I: Development of a model-based algorithm. *J. Appl. Meteor.*, **43**, 1095-1113.

Shige, S., Y. N. Takayabu, W.-K. Tao and C.-L. Shie, 2007: Spectral retrieval of latent heating profiles from TRMM PR data. Part II: Algorithm Improvement and heating estimates over tropical ocean regions. *J. Appl. Meteor.*, **46**, 1098-1124.

Siqueira, J. R., W. B. Rossow, L. A. T. Machado, and C. Pearl, 2005: Structural characteristics of convective systems over South America related to cold-frontal incursions. *Mon. Wea. Rev.*, **133**, 1045-1064.

Spencer, R. W., R. Hood, and M. Goodman, 1989: Precipitation retrieval over land and ocean with the SSM/I - Identification and characteristics of the scattering signal. *J. Atmos. Oceanic Technol.*, **6**, 254-273.

Takahashi, N., and T. Iguchi, 2004: Estimation and correction of beam mismatch of the precipitation radar after an orbit boost of the Tropical Rainfall Measuring Mission Satellite. *IEEE Trans. Geosci. Remote Sens.*, **42**, 2362-2369.

Takayabu, N. Y., S. Shige, W.-K. Tao, and N. Hirota, 2010: Shallow and deep latent heating modes over tropical oceans observed with TRMM PR spectral latent heating data. *J. Climate*, **23**, 2030-2046.

Tao, W.-K., and Coauthors, 2006: Retrieval of latent heating from TRMM measurements. *Bull. Amer. Meteor. Soc.*, **87**, 1555-1572.

Williams, M., and R. A. Houze, 1987: Satellite-observed characteristics of winter monsoon cloud clusters. *Mon. Wea. Rev.*, **115**, 505-519.

Yamamoto, M., F. Furuzawa, A. Higuchi, and K. Nakamura, 2008: Comparison of diurnal variations in precipitation systems observed by TRMM PR, TMI, and VIRS. *J. Climate*, **21**, 4011-4028.